Desalination xxx (2016) xxx–xxx

Contents lists available at ScienceDirect

Desalination

journal homepage: www.elsevier.com/locate/desal

Review on the energy and economic efficiencies of passive and active solar distillation systems

G.N. Tiwari [a], Lovedeep Sahota [b,*]

[a] Bag Energy Research Society (BERS), SODHA BERS COMPLEX, Plot No. 51, Mahamana Nagar, Karaundi Varanasi, UP 221005, India
[b] Centre for Energy Studies, Indian Institute of Technology Delhi, Hauz Khas, New Delhi 110016, India

HIGHLIGHTS

- Performance of different solar stills (passive/active) has been studied theroretically and experimently.
- Passive double slope solar stills perform better than passive single slope solar stills on the basis of productivity.
- Active single slope solar still (N PVT-FPC/N-PVT-CPC) performs better than the active double slope solar still (N PVT-FPC/N-PVT-CPC) above critical water depth on the basis of productivity and vice versa. At critical water depth, yield is approximately same.
- Use of water based nanofluids having better thermo-physical and optical properties improve the solar still productivity.

ARTICLE INFO

Article history:
Received 6 April 2016
Received in revised form 25 August 2016
Accepted 29 August 2016
Available online xxxx

Keywords:
Active solar still
Passive solar still
Nanofluids

ABSTRACT

Water is one of the prime elements responsible for life on the Earth. The demand of potable water is growing continuously due to its rapid use in agriculture, industry, and population. To overcome the challenge of water shortage, it is essential to minimize the gap among the demand and supply of potable water by developing alternative technologies of water purification. It is becoming a challenge to avail of low cost potable water to mankind. Solar distillation is one of the most promising, simple, and economic methodology for salt and brackish water purification by utilizing solar energy (renewable energy source). Worldwide, various researchers experimentally analyzed the performance of different types of solar stills and numerous research works has also been performed to develop the theoretical models based on energy balances. In present paper, experimentally and theoretically detailed work done in recent past on passive and active solar stills has been highlighted. System performance; exergoeconomic and enviroeconomic analysis; different solar still designs; and recent techniques in solar stills have been discussed in detail. Furthermore, a discussion on future scope of the work on solar stills for sustainable potable water production is given with some recommendations.

1. Introduction

Potable water is essential for all living organisms to survive on the Earth. The availability of potable water from the natural water resources is shrinking day by day due to rapid growth of population, poor water management and water pollution. Due to geography, climate, engineering, regulation, and competition for resources, most regions face drought of potable water supply. The inflation of water crisis would be controlled if we can effectively conserve, manage, and carefully distribute the available fresh water.

Today, it is the main challenge to fulfill the gap between demand and supply of potable water to make it available for all the creatures on the planet earth. Contaminated water usually contains bacteria, viruses, parasitical organisms, dissolved and undisclosed materials, chemical and physical contaminants which causes serious damage of health on consumption. Consequently, it is essential to find an alternate methods or techniques to purify the contaminated or filthy water (rain water, boring wells, rivers, lakes, oceans etc.) to avail low cost potable/fresh water. There are various high and medium technologies available for water purification viz. Multiple Effect Distillation (MED), Multi Stage Flash (MSF) desalination, Thermal Vapor Compression (TVC), Mechanical Vapor Compression (MVC), Reverse Osmosis (RO) and others. All these technologies depend on conventional source of energy (electricity) and require high-tech parts i.e. batteries, filters or membranes etc. On the other hand, solar distillation is the simplest, cost effective, and environment friendly technology for water purification. The classification of solar desalination methods has been illustrated in Fig. 1(a).

Solar desalination is one of the popular treatment solutions throughout the world. Solar distiller or simply solar stills produce pure water by

* Corresponding author.
E-mail address: gntcesiitd@gmail.com (L. Sahota).

http://dx.doi.org/10.1016/j.desal.2016.08.023
0011-9164/

using non-conventional source or renewable energy resource (solar energy). Solar stills are classified into two categories viz. passive and active solar stills as shown in Fig. 1(b). Among all solar stills, the most simple and least expensive are the conventional single slope and double slope systems. Solar stills can to purify contaminated water containing salt concentration up to 10^4 ppm (part per million).

In the historical review on desalination of water, Nebbia and Menozzi [1] mention the historical background of solar distillation. Later, Malik et al. [2] reveals the historical background of solar distillation systems in their book and investigated the work on passive solar distillation. Garg and Mann [3] studied the effect of climatic, operational, and design parameters on annual performance of single and double slope solar still for Indian arid zone conditions. The performance of basin type solar still integrated with flat plate collector was first time studied by Soliman [4]. Later Rai and Tiwari [5] studied the performance of single basin solar still integrated with flat plate collector. They perceived good enhancement in the system yield in comparison to the conversional single slope solar still. Sodha et al. [6] presented the design of a multiple wick solar still and analyzed its performance. The high temperature on account of minimum thermal capacity has been attained through the blackened wet jute cloth (liquid surface) and the system has been oriented to retrieve the maximum solar radiation. The system performance further can be improved by incorporating double condensing cover [7]. Tiwari and Garg [8] studied various designs of solar distillation systems. Long term performance of various designs has also been analyzed by Tiwari and Yadav [9]. They conclude that the performance

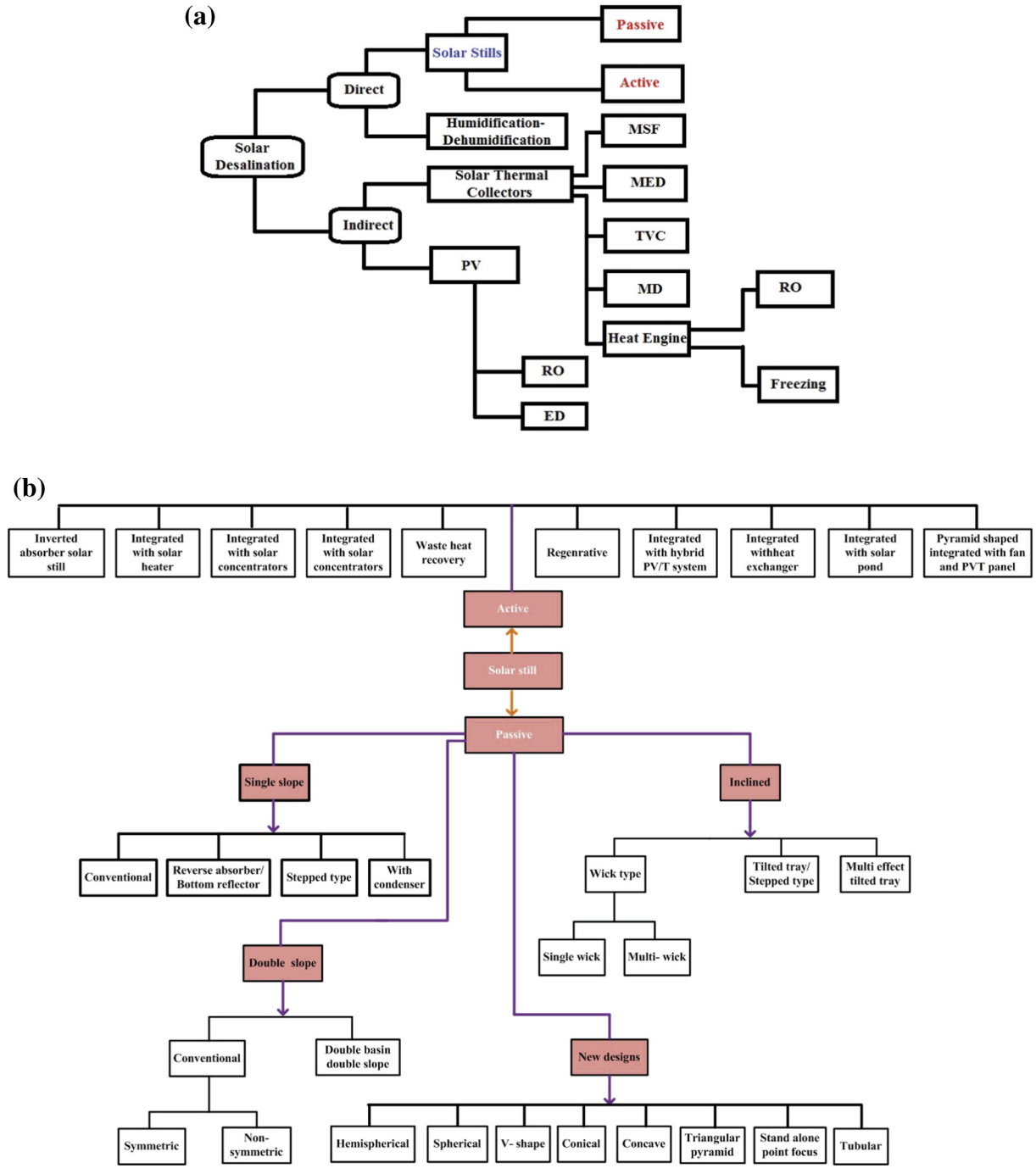

Fig. 1. (a) Classification of solar desalination process. (b) Various designs of active and passive solar stills.

Please cite this article as: G.N. Tiwari, L. Sahota, Review on the energy and economic efficiencies of passive and active solar distillation systems, Desalination (2016), http://dx.doi.org/10.1016/j.desal.2016.08.023

of a single slope solar still is better than a double slope solar still for cold climatic conditions, and a double slope solar still gives better performance than a single slope solar still for summer climatic conditions. Lawrence and Tiwari [10] theoretically analyzed the performance of single slope solar distillation system integrated with panel of collectors under natural circulation mode with heat exchanger. They conclude that natural circulation mode has many advantages over the forced circulation mode in terms of reliability, cost effectiveness, and simplicity. Tayeb [11] analyzed the performance of four different designs of basin type solar stills having same basin area.

Basically, the performance solar distillation system depends on climatic conditions and various other parameters such as inclination angle of the glass cover, water depth in the basin, orientation, vapor tightness, dimensions and body of the still etc. The system can be improved further by enhancing the internal heat transfer modes, temperature difference among the basin water and the inner surface of the condensing cover [12–16].

The internal heat and mass transfer mechanism of passive solar stills is critically presented by Tsilingiris [17–20]. He critically analyzed impact of binary mixture thermo-physical properties in processes of heat and mass transfer. He developed a model for heat and mass transfer processes for the distillation systems functioning at high temperature range. Later, he investigated the accuracy and validity range of earlier developed theories of heat and mass transfer within the still cavity. Furthermore, he examined expressions of a group of mass transfer coefficients on the basis of Bowen's ratio as applied on properly modified diffusive interface model under specific assumptions. Dwivedi and Tiwari [21] investigated the experimental validation of internal heat transfer coefficients in single and double slope passive solar stills for different water depths using different thermal models.

Furthermore, it is essential to analyze the solar distillation systems from the economic aspects. Use of solar stills in place of conventional energy (electricity) dependent distillation systems reduces the effect of inflation on unit costs of conventional sources. In literature, various researchers studied the economic analysis of solar distillation systems. Govind and Tiwari [22] presented the cost analysis of solar dryers, solar water heating systems and solar distillation units by considering various factors. Later, Mukherjee and Tiwari [23] investigated the economic analysis of various designs of conventional solar stills. They have presented the cost analysis of a single slope fibre reinforced plastic (FRP) still, a double-slope FRP still and a double slope concrete still. On the basis of annual performance, the life cycle cost analysis of single slope hybrid photovoltaic thermal active solar still is studied by Kumar and Tiwari [24]. Further, Liu et al. [25] studied the thermal and economic analyses of solar desalination system coupled with evacuated tubular collectors. El-Baily et al. [26] studied the cost analysis of several active and passive solar distillation systems in detail. From the literature, it has been concluded that the passive solar distillation systems are more economic in comparison to the active. Single slope passive solar stills perform better than double slope passive solar stills on the basis of annual yield, annual energy, annual exergy and exergoeconomic parameter.

In present decade, various researchers studied different new designs of passive (step-basin, multi-basin, hemispherical, spherical, V-shape, concave, tubular, triangular pyramid, inclined wick type, stand alone, tubular etc.) and active solar stills to enhance the system performance [27–46]. Kumar et al. [47] presented the review on different designs of passive and active solar stills. Thermal models of various designs of solar stills are presented by Elango et al. [48] in their comprehensive review.

In present paper, the detailed experimental and theoretical work carried out on passive and active solar stills in past few years has been emphasized. The performance of different solar stills on the basis of heat transfer coefficients; cost analysis; exergoeconomic and enviroeconomic analysis; characteristic curves have been discussed. The present paper also highlighted in details the other different designs and recent techniques to improve the solar still performance.

2. Passive solar stills

Schematic view and experimental setup of passive single slope solar still (SSSS) and double slope solar still (DSSS) are shown in Fig. 2 and Fig. 3. Body of the still is fabricated with fibre reinforce plastic (FRP) with a top transparent glass (3 − 4 mm) cover. Passive single slope solar still is facing due south and double slope is kept in east-west direction to retrieve maximum solar radiation (northern-hemisphere). Inner surface of the still basin is painted mat black (blackened surface/basin liner) to absorb maximum solar radiation.

Fraction of solar radiation has been reflected from the outer surface of the top cover and water surface, maximum solar radiation penetrates into the still and gets absorbed in water and basin liner. Various components of energy balance and thermal energy losses in passive SSSS and DSSS systems are shown in Fig. 2(a) and (b) respectively. The attenuation of solar flux through the water mass depends critically on the quantity of basin water and its absorptivity. Most of the solar radiation reaches the basin liner and get absorbed there. Further, stored thermal energy in the basin liner is convected to the water mass and raises the water temperature. Consequently, the temperature difference among the evaporative surface and inner surface of the glass cover increases which acts as a driving force for the enhanced system yield. Heat transfer mechanism takes place in the still cavity and evaporated water reaches on the inner surface of the glass cover. It condensed there after releasing its latent heat to the glass cover. The condensed water trickles into the channels provided at the lower ends of the glass cover under gravity [49].

2.1. Heat transfer coefficients (HTCs) in passive single slope solar still (SSSS) and double slope solar still (DSSS) [21]

Dwivedi and Tiwari [21] estimated the internal heat transfer coefficients of passive single slope and double slope solar still for 15-^{0} inclination of the glass cover and three different water depths (0.01, 0.02 and 0.03 m) for summer and winter climatic conditions.

Different thermal models (Table 1) reported in literature have been validated with the experimental results of the system yield for the composite climate of New Delhi(28°35′N). The hourly variation of evaporative HTCs of the passive single slope and double slope (east and west side) solar still is shown in Fig. 4. It has been perceived that Kumar and Tiwari; Dunkle; and Chen et al. models give better correlation among the theoretical and experimental results of the hourly yield. Clark's model predicts lower values as compared with the experimental results whereas the yield obtained using Adhikari and Zheng et al. model is very high. Furthermore, the overall annual yield of the passive SSSS is found to be higher (499.41 l/y) as compared to the DSSS (464.68 l/y).They have conclude that Dunkle's model can be used for lower water depth (0.01 – 0.03 m) to determine the internal HTCs. Basically, the productivity represents the relationship between output and the factors used in achieving the output. Its objective is to get output as high as possible with less and less input of resources. It is the ratio of effectiveness and efficiency as defined by ILO [107]. Singh et al. [106] studied the life cycle cost analysis of conventional single slope and double slope passive solar stills with energy matrices. They concluded that passive double slope solar stills perform better than passive single slope solar stills on the basis of productivity because annual yield for double slope is lower than single slope by 11.78% and uniform end-of-year annual cost is lower for the same by 16.52%. The equation of productivity of the solar distillation system is given below as;

$$\text{Productivity } [105] = \frac{M_{ew} \times (SP)_w}{UAC} \times 100$$

where, M_{ew} represents the annual yield, $(SP)_w$ represent the selling price of water and *UAC* represents the uniform end-of-year annual cost.

Please cite this article as: G.N. Tiwari, L. Sahota, Review on the energy and economic efficiencies of passive and active solar distillation systems, Desalination (2016), http://dx.doi.org/10.1016/j.desal.2016.08.023

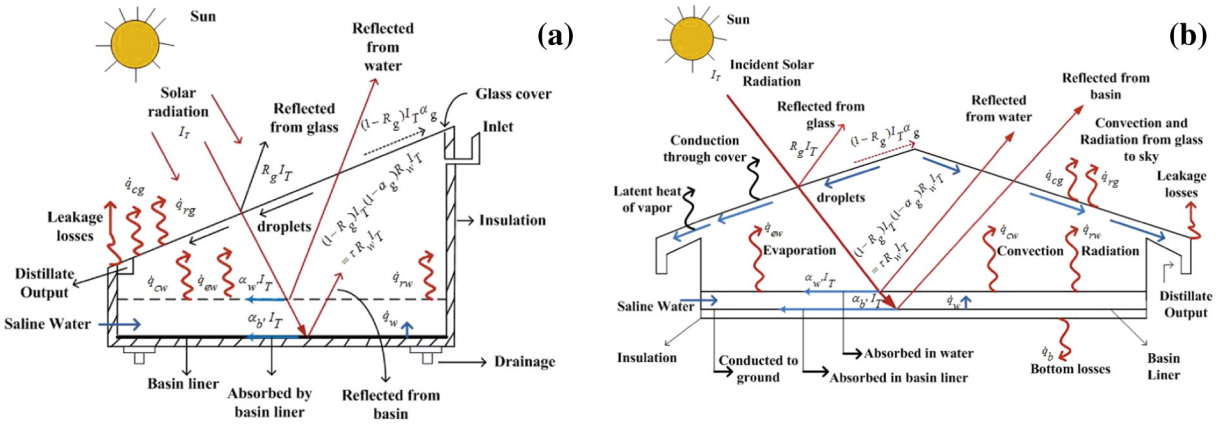

Fig. 2. Systematic view of (a) passive single slope and (b) double slope solar still.

It means that the percentage decrease in denominator is more than numerator of the productivity equation and hence ratio is higher for double slope than single slope passive solar still. The variation annual productivity (η_p) and of exergoeconomic parameter (Rg_{ex}) with rate of interest for 30 year life time for single slope and double slope passive solar still is shown in Fig. 5. The value of M_{ew} depends on the product of evaporative heat transfer coefficient and temperature difference between evaporative surface and inner surface of the glass cover (T_{gi}). If ambient temperature is lower, then T_{gi} will be lower due to increase in the rate of heat transfer among the glass surface and ambient which results in the increase in the temperature difference of T_w and T_{gi}. Hence, yield will increase with the decrease in ambient temperature and vice-versa. Further, if solar intensity increases then evaporative heat transfer coefficient increases which is clear from Fig. 6(a) and (b). Hence, yield increases with the increase in solar intensity.

2.2. Characteristic equation of passive solar stills

Efficiency is an essential parameter to understand the performance of the solar stills. The optimal distillate from the designed still needs to investigate the different parametric studies i.e. inclination of glass cover, ambient temperature, wind velocity, feed water temperature, salinity, water depth and other effects like heat transfer coefficients, influence of binary mixture thermo-physical properties, effect of thermal storage, solar intensity and symmetry-asymmetry of design of passive solar still. Therefore, the concept of efficiency is vital for designing and improving the solar still performance. These characteristic equations can be used for further modifications in the existing design in terms of design (i.e. size, angle of inclinations of condensing glass covers, and material), operating (i.e. water depth, mode of operation, shading on condensing covers and use of dye) and climatic factors (i.e. location of the place, input amount of solar radiation, ambient temperature, and wind velocity) etc.

2.2.1. Characteristic equation of passive single slope solar still (SSSS) [55]

Schematic diagram of passive single slope solar still (SSSS) is shown in Fig. 2 (a). To generate the linear and non-linear characteristic equation for of three different inclination angles (15°, 30°, and 45°) of the glass cover, Dev and Tiwari [55] used the characteristic equation different climatic conditions (summer and winter) of New Delhi. For better understanding of the solar still performance, the instantaneous gain and loss efficiency curves have been simultaneously analyzed by Dev and Tiwari.

Following Dev and Tiwari [55], the temperature of basin water can be expressed as

$$T_w = \frac{\overline{f'(t)}}{a}\left[1-e^{-a\Delta t}\right] + T_{w0}\, e^{-a\Delta t} \tag{1}$$

The rate of evaporative heat transfer can be expressed as

$$\dot{q}_{ew} = h_{ew}(T_w - T_{gi}) = \frac{h_{ew}U_{cg-a}}{h_{1w}+U_{cg-a}}(T_w - T_a) \tag{2}$$

Substituting Eq. (1) in Eq. (2), and simplifying,

$$\dot{q}_{ew} = \frac{1}{U_L}\left(\frac{h_{ew}U_{cg-a}}{h_{1w}+U_{cg-a}}\right)\left[\alpha_e\left(1-e^{-a\Delta t}\right)I(t) + U_L e^{-a\Delta t}(T_{w0}-T_a)\right] \tag{3}$$

Instantaneous thermal efficiency can be expressed as

$$\eta_i = \frac{\dot{q}_{ew}}{I(t)} = F'(\alpha\tau)_{eff} + F''(U)_{eff}\frac{(T_{w0}-T_a)}{I(t)} \tag{4}$$

It clearly express that the upward rate should be maximum for better performance of solar still (positive slope of the curve).

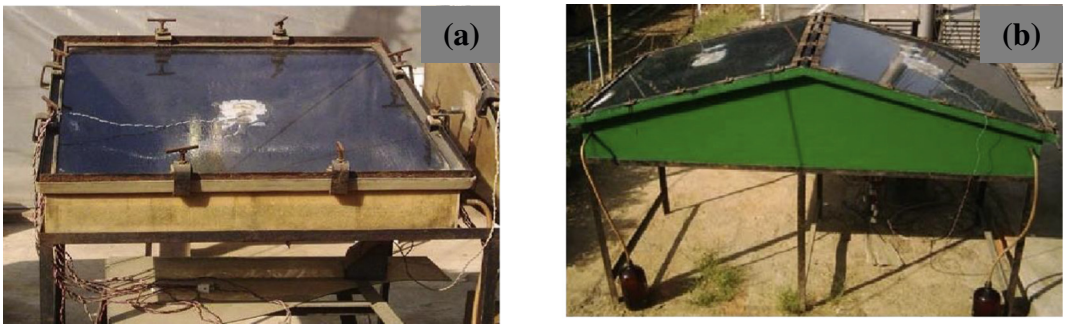

Fig. 3. Experimental setup of (a) single slope and (b) double slope passive solar still.

Please cite this article as: G.N. Tiwari, L. Sahota, Review on the energy and economic efficiencies of passive and active solar distillation systems, Desalination (2016), http://dx.doi.org/10.1016/j.desal.2016.08.023

Further, the instantaneous loss efficiency can be expressed as

$$\eta_{iL} = \frac{M_w C_w (T_w - T_{wo})}{I(t)} = F' \left[\alpha_e - U_L \frac{(T_w - T_a)}{I(t)} \right] \quad (5)$$

For higher instantaneous gain efficiency of the still, the instantaneous loss efficiency should be lower in Eq. (4).

The unknowns in Eq. (4) and Eq. (5) are given in Appendix A [55].

Dev and Tiwari observed that the system gives better performance for 45° inclination of the glass cover for summer conditions (Fig. 7). There is enhancement in instantaneous efficiency for 30° and 45° inclination of the glass cover but reduced for 15° inclination angle.

Linear characteristic equations indicate that the coefficient $F'Ue^{-a\Delta t}$ is higher for a solar still for 45° inclination angle of the glass cover in comparison to the other inclination angles. Therefore, it results in more heat input in the solar still. Linear characteristic equations imply that the coefficient $F'Ue^{-a\Delta t}$ is lowest at higher basin water depths due to heat storage effect. The instantaneous gain efficiency at lower basin water depths has been found higher. It has been concluded that the optimized inclination angle of the glass cover of the solar still is 45° from the design point of view.

2.2.2. Characteristic equation of passive double slope solar still (DSSS) [56]

Illustrative view of passive double slope solar still is shown in Fig. 2(b). On the basis of experimental observation Dev et al. [56] evaluated the characteristic equation of passive DSSS system for the composite climatic condition of New Delhi, India. Following Tiwari and Noor [57], the instantaneous gain can be expressed as

$$\eta_i = \frac{h_{ew}(T_w - T_{gi})}{I(t)} = (\alpha\tau)_{eff} + U' \frac{\{(T_{w0} - T_a)/I(t)\}}{\{(T_{w0} - T_a)/I(t)\}_{max}} \quad (6)$$

Instantaneous loss efficiency can be expressed as

$$\eta_{iL} = \left[(\alpha\tau)_{EFF} - U_L \frac{(T_{w0} - T_a)}{I(t)} \right] \text{ Or } \eta_{iL} = \left[(\alpha\tau)_{EFF} - U'' \frac{\{(T_{w0} - T_a)/I(t)\}}{\{(T_{w0} - T_a)/I(t)\}_{max}} \right] \quad (7)$$

The unknowns in Eq. (6) and Eq. (7) are given in Appendix A [56].

It has been perceived that non-linear characteristic curves give better results in comparison to the linear characteristic curves on analyzing the performance, thermal testing and further design modification of the system. Furthermore, under quasi-steady state condition, the coefficient of correlations is higher for non-linear characteristic curves in comparison to the linear characteristic curves. The characteristic equations of both sides of the top transparent glass cover are different which can be used to determine or optimize the inclination angle of the transparent glass cover for better performance of the passive DSSS.

Table 1
Thermal models of internal heat transfer coefficients (HTCs).

Thermal models	Relations
Kumar and Tiwari [51]	$(Nu)_w = \frac{hX}{k} = C(GrPr)^n$
	Grashof number $(Gr)_w = \left[\frac{g\beta\rho^2 L^3 \Delta T}{\mu^2}\right]_w$
	Prandtl number $(Pr)_w = \left(\frac{\mu C_p}{k}\right)_w$
	Rayleigh number $(Ra)_w = (GrPr)_w = \left[\frac{g\beta\rho^2 C_p L^3 \Delta T}{\mu k}\right]_w$
	C = 0.54 and n = ¼ horizontal plate facing upward
Chen et al. [52]	$h_{cw} = 0.2Ra^{0.26}\frac{K_v}{X_v}$
	Remarks: For a wide range of Rayleigh number $(3.5\times10^3 < Ra < 10^6)$
Adhikari et al. [53]	Yield; $\dot{m} = \alpha(\Delta T)^n (P_w - P_{gi})$
	$n = \begin{cases} 1/3 \text{ for } 2.51\times10^5 < Gr < 10^7 \\ 1/4 \text{ for } 10^4 < Gr < 2.51\times10^5 \end{cases}$
Zheng at al. [54]	$h_{cw} = 0.2Ra^{0.26}\frac{K_v}{X_v}$
	$\Delta T = (T_w - T_{gi}) + \left[\frac{(P_w - P_{gi})(T_w + 273)}{M_{aP_t}/(M_a - M_w) - P_w}\right]$

2.2.3. Characteristic equation of the inverted absorber solar still (IASS) [58]

Experimental setup and systematic view of inverted absorber solar still (IASS) are shown in Fig. 8(a) and (b) respectively. In IASS system, reflector has been kept underneath the solar still to heat up the basin from the bottom side in addition to direct heating of the basin. Consequently, higher water temperature is achieved in comparison to the conventional single slope solar still. An experimental setup of the IASS system has been installed at Solar Energy Laboratory, Sultan Qaboos University, Muscat, Oman (latitude 23° 37′ N, longitude 58° 35′ E). The characteristic equation of the IASS and SSSS system has been developed for three different water depths (0.01 m, 0.02 m, and 0.003 m) on the basis of experimental data.

Following Dev and Tiwari [58], energy balances of different components of the IASS system are expressed as

(i) Absorber basin plate

$$(\tau_g\tau_w)\alpha_b I(t) + (r_{inv}^N)\alpha_b I(t) = h_{cpw}(T_{bu} - T_w) + U_r(T_{bu} - T_a) \quad (8)$$

(ii) Water mass

$$h_{cpw}(T_{bu} - T_w) = M_w C_w \frac{dT_w}{dt} + h_{1w}(T_w - T_{gi}) \quad (9)$$

(iii) Condensing glass cover

$$h_{1w}(T_w - T_{gi}) + \frac{K_g}{L_g}(T_{gi} - T_{go}) = h_0(T_{go} - T_a) = h_{go}(T_{gi} - T_a) \quad (10)$$

On solving Eqs. (8)–(10), one can get

$$T_w = \frac{\overline{f'(t)}}{a}\left[1 - e^{-a\Delta t}\right] + T_{w0}\, e^{-a\Delta t} \quad (11)$$

Instantaneous thermal efficiency can be expressed as

$$\eta_i = \frac{h_{ew}(T_w - T_{gi})}{2 \times I(t)} = F'(\alpha\tau)_{EFF}\left(1 - e^{-a\Delta t}\right) + F'U_L e^{-a\Delta t}\frac{(T_{w0} - T_a)}{I(t)} \quad (12)$$

Similarly, instantaneous loss efficiency can be expressed as

$$\eta_{iL} = \frac{M_w C_w (T_w - T_{wo})}{2 \times I(t)} = F'' \left[(\alpha\tau)_{EFF} - U_L \frac{(T_{w0} - T_a)}{I(t)} \right] \quad (13)$$

The unknowns in Eq. (12) and Eq. (13) are given in Appendix A [58].

The variation of instantaneous gain and loss efficiency curves of the IASS system with reduced mass at different water depths under quasi steady condition is shown in Fig. 9. It clearly shows that the behavior of the IASS and SSSS system has been expressed better by the non-linear characteristic curves. It is credited to the non-linearity in the climatic parameters. The instantaneous thermal efficiency of SSSS system found to be higher in comparison to the IASS system for the same parameters. It decreases with increase in basin water depth whereas the instantaneous loss efficiency decreases due to the water thermal storage effect.

2.3. Instantaneous exergy efficiency of a shallow basin passive solar still [59]

It has been reported that the maximum annual yield from the solar still strongly depends on latitude and glass cover tilt angle. Furthermore, deterioration of absorber liner decreases the effective absorptivity of basin liner. Therefore, it is necessary to investigate instantaneous exergy efficiency of the passive solar still in terms of design and climatic parameters; and to analyze the relative influence of basin water temperature

Please cite this article as: G.N. Tiwari, L. Sahota, Review on the energy and economic efficiencies of passive and active solar distillation systems, Desalination (2016), http://dx.doi.org/10.1016/j.desal.2016.08.023

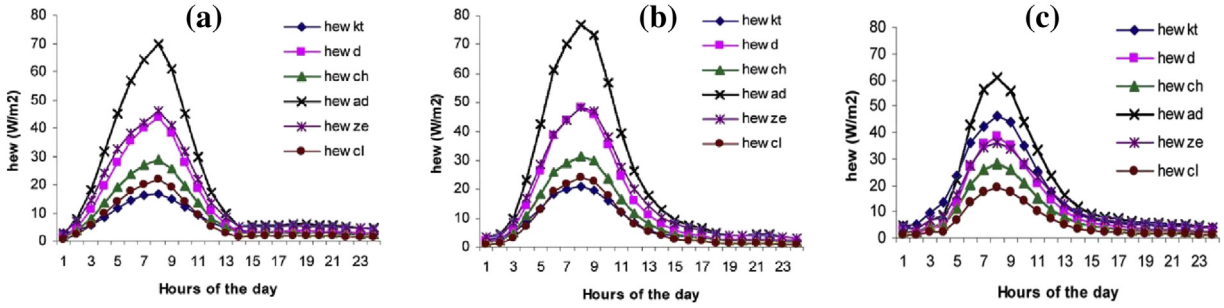

Fig. 4. Hourly variation of evaporative HTC of passive (a) single slope, (b) east side of double slope and (c) west side of double slope solar still using different thermal models.

on the fractional exergies. Also, it is important to find the effect of various parameters viz. effective absorptivity, glass cover tilt, water depths, and wind velocity on instantaneous energy and exergy efficiency.

Kumar and Tiwari [59] analyzed the instantaneous exergy efficiency of passive solar still. The effect of various parameters viz. absorptivity of the basin liner (0.6 − 0.9), inclination (15° − 45°) the glass cover, and wind velocity (0 − 10 m/s) on instantaneous energy and exergy efficiency has been analyzed. Following Kumar and Tiwari, instantaneous exergy efficiency can be expressed as

$$\epsilon_i = \frac{\dot{E}_{\chi,evap}}{\dot{E}_{\chi,sun}} = \eta_i \frac{(T_w - T_a)}{T_w\left[1 - \frac{4}{3}\left(\frac{T_a}{T_s}\right) + \frac{1}{3}\left(\frac{T_a}{T_s}\right)^3\right]} = (1.017\,\eta_i)\left(1 + \frac{h_{eff}T_a}{I_s(t)\eta_i}\right)^{-1} \quad (14)$$

Above equation represents the instantaneous exergy efficiency of passive solar still. The unknowns are given in Appendix [59].

The rate of exergy transfer (evaporation, convection, and radiation) within the still cavity can be expressed as

$$\dot{E}_{\chi,evap} = h_{ew}(T_w - T_{gi})A_b\left(1 - \frac{T_a}{T_w}\right) \quad (15)$$

$$\dot{E}_{\chi,cw} = h_{cw}(T_w - T_{gi})A_b\left(1 - \frac{T_a}{T_w}\right) \quad (16)$$

$$\dot{E}_{\chi,rw} = h_{rw}(T_w - T_{gi})A_b\left[1 - \frac{4}{3}\left(\frac{T_a}{T_s}\right) + \frac{1}{3}\left(\frac{T_a}{T_s}\right)^3\right] \quad (17)$$

The dominant mode of rate of exergy transfer can be understood from the fraction of total exergy. The fraction of rate of exergy transfer

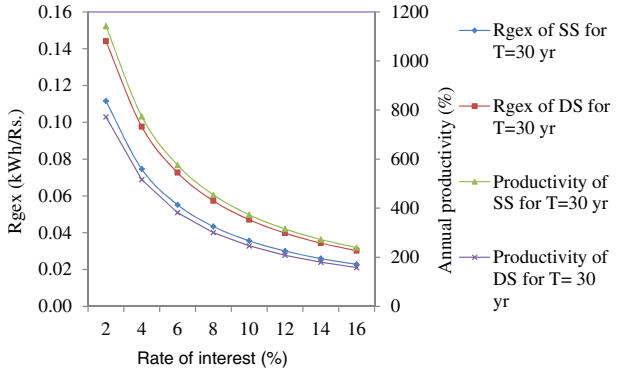

Fig. 5. Variation of exergoeconomic parameter (R_{gex}) and annual productivity (η_p) with rate of interest for 30yr life time for single slope and double slope passive solar still [106].

of all three modes in the still cavity can be expressed as

$$F_{e\chi} = \frac{\dot{E}_{\chi,evap}}{\dot{E}_{\chi,t}};\ F_{c\chi} = \frac{\dot{E}_{\chi,cw}}{\dot{E}_{\chi,t}};\ F_{r\chi} = \frac{\dot{E}_{\chi,rw}}{\dot{E}_{\chi,t}} \quad (18)$$

From the analysis, it has been perceived that the enhancement in absorptivity raises the energetic and exergetic efficiencies of the system. The variation of instantaneous energy and exergy efficiency with inclination of the glass cover and wind speed is shown in Fig. 10(a) and Fig. 10(b) respectively. It has been observed that the instantaneous energy and exergy efficiency varies between 5.4–54.8% and 0.4–10.7% respectively. The effect of inclination angle of the glass cover has been found insignificant on the energy and exergy efficiencies whereas it enhances significantly on increasing the wind speed. The variation of fraction exergy with water mass [59] reveals that the evaporative exergy fraction and efficiency increases significantly with increase in the water temperature (Fig. 10(c)). Furthermore, evaporative exergy fraction found to be higher than the radiative and convective exergy fractions above 30^0 (>50%) which have been found to be the more suitable conditions to operate the solar still.

3. Active solar still

The efficiency of solar still can be improved with force circulation mode of operation. In force circulation mode, the temperature of water in the still can be elevated. Consequently, the temperature difference among the evaporative surface (water) and inner surface of the glass cover can be increased which acts as a driving force for distillation process.

Either conventional or non-conventional external source of energy is required to raise the water temperature. Force mode of operation is achieved by using pump which can further run either by conventional source of energy (electricity) or non-conventional source of energy (Photovoltaic, PV). Therefore, integration of solar still with solar thermal technology (flat plat collator (FPC), evacuated tubular collector (ETC), compound parabolic concentrator (CPC)) and photovoltaic technology to fulfill the external energy requirement makes it photovoltaic thermal (PVT) active solar still.

The PV modules generates the electrical energy and supplied it to the DC motor water pump which circulates the basin water under the forced mode of operation and thus overcomes the pressure drop in collectors and flow channels. The fluid passing through the pipe in the collector gets heated after receiving the thermal energy from the blackened surface of the collector (absorbs the incident solar radiation), the thermal energy convected from the back surface of the PV module and solar radiation being transmitted through non packing area of module. Hence, force mode of operation is achieved by using pump which can further run either by conventional source of energy (electricity) or non-conventional source of energy (Photovoltaic, PV).

Experimental setup and a cross section view of an identical photovoltaic thermal flat plate collector (PVT-FPC) integrated with single

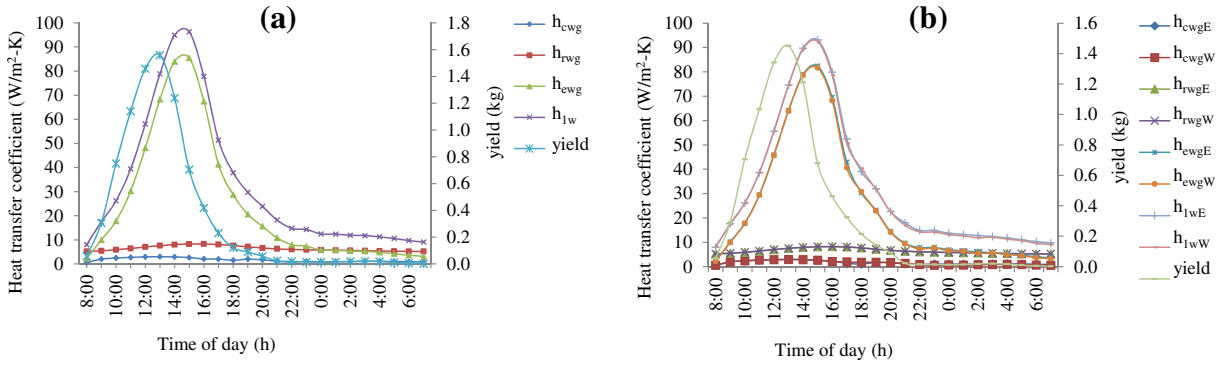

Fig. 6. Hourly variation of heat transfer coefficient and yield for (a) single slope and (b) double slope passive solar still for a typical day in the month of May [106]

slope solar still is shown in Fig. 11(a) and (b)respectively. The system mainly consists of three components viz. solar still, DC motor, and partially covered PVT-FPC. The collector is the heart of any solar energy collection system designed for functioning in the low (ambient-60 °C) or the medium temperature range (ambient-100 °C). The collector absorbs the maximum solar energy (beam and the diffuse radiation) and gets heated, which later transfer that heat to a stream of liquid or gas. The FPC consists of glazing; tubes and fins; absorber plate; heads and manifolds; insulation; and casing. Among all, the absorber plate is the most essential part of the collector. The liquid or air flowing through the duct or pipe which is in thermal contact along with the absorber plate transfers heat to it. The surface of the plate is coated to enhance the absorptivity (minimize the emissivity) and ultimately to obtain the required range of temperature.

The solar still in the system is fabricated with fibre reinforced plastic (FRP) and the inner surface of the still is painted black (blackened surface) to raise the absorptivity of the still as explained earlier. The solar still and the PVT-FPC are facing due south to retrieve the maximum solar radiation in northern-hemisphere. The still from the top is covered with a transparent glass cover of thickness (3 − 4 mm). The basic mechanism of distillation in active solar still is similar to the passive case as discussed earlier in Section 2.

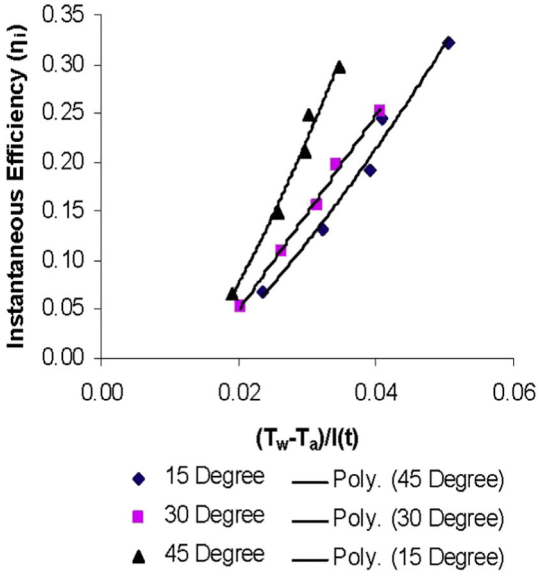

Fig. 7. Polynomial characteristic curves of passive single slope solar still for different inclination angles of the glass cover at 0.04 m water depth.

3.1. Internal heat transfer coefficients (HTCs) of a hybrid (PVT) active solar still

As discussed earlier, the main motive o coupling the PVT-FPC system with the solar still is to raise feed the external thermal energy into the solar still basin. Ultimately, it will increase the rate of evaporation rom the water surface within the still cavity. Kumar and Tiwari [60] estimated the internal heat transfer coefficients of single slope deep basin solar still coupled with photovoltaic thermal (PV/T) system (Fig. 11(a) and (b)) for the composite climate of New Delhi, India. They evaluated the annual yield and internal HTCs using different thermal models (Table 1) proposed by various researchers and compares the results with experimental one. In the model development (Kumar and Tiwari model), the still cavity size, temperature range of operation and inclination of the glass cover and its position have been considered. On the basis of experimental data, the consents C and n has been evaluated using regression analysis.

The Nusselt number (Nu) for natural convective HTC can be expressed as

$$(Nu)_w = \frac{h_{cw}X_v}{K_v} = C(GrPr)^n \text{ Or } h_{cw} = C(GrPr)^n\frac{K_v}{X_v} \tag{19}$$

The distillate output from the system can be expressed as

$$\frac{\dot{m}_w}{K} = C(GrPr)^n; \text{where } K = (0.016273)\frac{K_v}{X_v}\left[\frac{P_w - P_{gi}}{T_f - T_{gi}}\right] \tag{20}$$

Taking log on both sides of the above equation and comparing it with straight line equation, one can get;

$$y = \ln\left(\frac{\dot{m}_w}{K}\right); C_0 = \ln C; x = \ln(Gr.Pr); \text{and } m = n \tag{21}$$

m and C_0 can be obtained by using linear regression analysis.

After knowing the values of m and C_0 for the N number of observations, the constants C and n can be evaluated from Eq. (21). The precision of fitting of the diverse models can be computed by the correlation coefficients (r) whereas the percentage deviation (e) measures accuracy of the results. The expressions of correlation coefficients (r) and percentage deviation (e) are given as

$$r = \frac{N\sum X_iY_i - (\sum X_i)(\sum Y_i)}{\sqrt{N\sum X_i^2 - (\sum X_i)^2}\sqrt{N\sum Y_i^2 - (\sum Y_i)^2}} \tag{22}$$

$$e = \left(\frac{X_i - Y_i}{X_i}\right) \times 100 \tag{23}$$

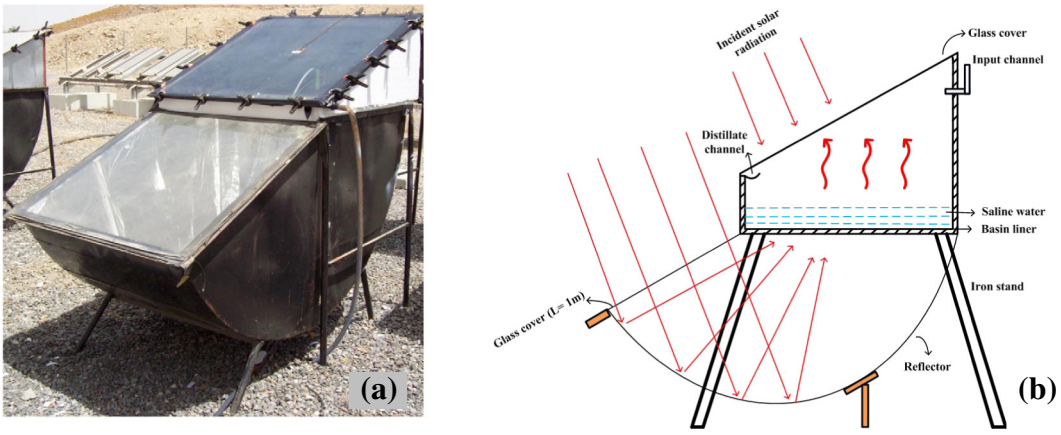

Fig. 8. (a) Experimental setup and (b) schematic view of inverted absorber solar still (IASSS).

The monthly average variation of convective and evaporative HTCs of passive and hybrid active system for fixed basin water depth is shown in Fig. 12. It has been observed that the KT model gives better results of convective HTCs in comparison to the Dunkle's model even for the water temperature range 24–55 °C. Except extreme cases, under the least percentage deviation consideration, the KT model is superior to the others model on the basis of hourly yield. The values of *C* and *n* is different depends on the system design and operating range of water temperature. For a typical day, the percentage deviation in total yield using Dunkle's model (22.7%, 35.7%, 27.7% and 59.8%) has been found to be higher than the KT model (27.2%, 29.6%, 20.2% and 45.5%). Eventually, the KT model gives better results in comparison to the other thermal models. It is more realistic for extensive water temperature range.

3.2. Development of empirical relation for basin type hybrid (PVT) active solar still [61]

Kumar et al. [61] developed empirical relation for the hybrid (PV/T) active solar still. They performed an experimental for a typical day of the month April 2006 of New Delhi (India) climatic conditions. They established linear and the non-linear correlation for the external radiative and total internal HTCs respectively. From these correlations, the semi-empirical equation has been developed to predict the glass cover temperature. The estimated theoretical results have been validated with the numerical solutions as well as with the experimental results.

Following Kumar et al. [61], the internal HTCs and temperature of the glass cover can be obtained as follows:

The radiative and convective HTCs can be expressed as

$$h_{rg} = \varepsilon_g \sigma \frac{\left(T_{go}^4 - T_a^4\right)}{(T_{go} - T_{sky})} + \varepsilon_g \frac{\Delta R}{(T_{go} - T_{sky})} \tag{24}$$

$$h_{cg} = h_w \frac{(T_{go} - T_a)}{(T_{go} - T_{sky})} \tag{25}$$

Therefore, total external HTC among the glass cover and sky (atmosphere) can be expressed as

$$h_{go} = \varepsilon_g \sigma \frac{\left(T_{go}^4 - T_a^4\right)}{(T_{go} - T_{sky})} + \varepsilon_g \frac{\Delta R}{(T_{go} - T_{sky})} + h_w \frac{(T_{go} - T_a)}{(T_{go} - T_{sky})} \tag{26}$$

Total internal HTC among the water and inner glass surface inside the still cavity is

$$h_{1w} = h_{ew} + h_{cw} + h_{rw} \tag{27}$$

where, $h_{ew} = (0.016273) h_{cw} \left[\frac{P_w - P_{gi}}{T_w - T_{gi}}\right]$; $h_{cw} = (0.844)\left[(T_w - T_{gi}) + \left(\frac{(P_w - P_{gi})(T_w + 273)}{2.689 \times 10^5 - P_w}\right)\right]^{1/3}$; and $h_{rw} = \varepsilon_{eff} \sigma (T_w^2 + T_{gi}^2)(T_w + T_{gi})$;

The evaporative, convective, and radiative energy fractions can be expressed as

$$F_{ew} = \frac{\dot{q}_{ew}}{\dot{q}_{1w}}; F_{cw} = \frac{\dot{q}_{cw}}{\dot{q}_{1w}}; \text{and } F_{rw} = \frac{\dot{q}_{rw}}{\dot{q}_{1w}} \tag{28}$$

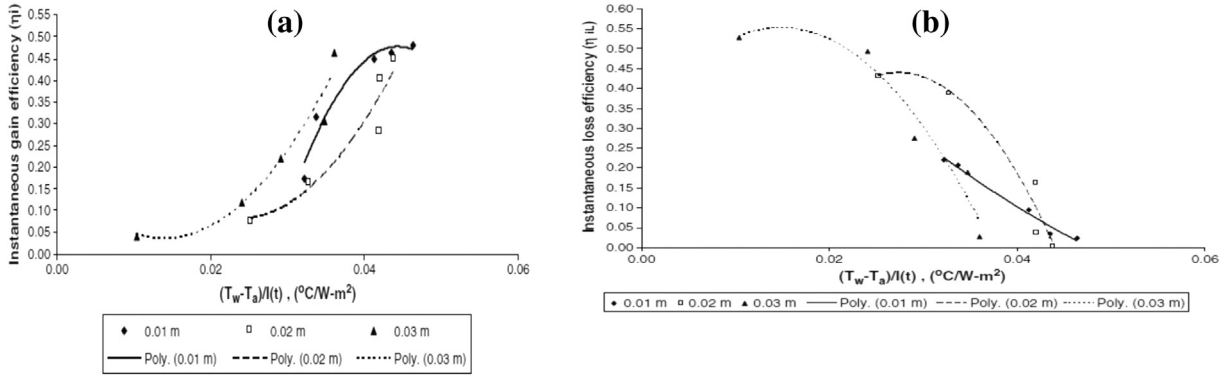

Fig. 9. Non-linear (a) instantaneous gain and (b) instantaneous loss efficiency of IASS at different water depths.

Please cite this article as: G.N. Tiwari, L. Sahota, Review on the energy and economic efficiencies of passive and active solar distillation systems, Desalination (2016), http://dx.doi.org/10.1016/j.desal.2016.08.023

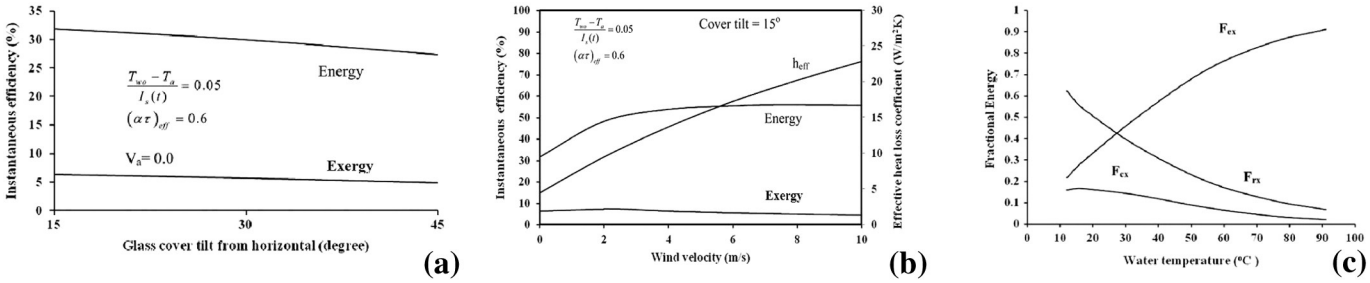

Fig. 10. (a) The variation of instantaneous energy and exergy efficiency of the still with glass cover inclination angle, (b) the variation of instantaneous energy and exergy efficiency and effective heat loss coefficient with wind speed, (c) the variation of exergy fraction with water mass in the still.

The higher value of the evaporation energy fraction means that the evaporation rate is higher from the water surface. On the other hand, higher convective energy fraction implies the faster the transfer of water vapors from the water surface. Therefore, for better efficiency of the system, both these fractions need to be higher. The energy balance equation of the glass cover can be expressed as

$$\varepsilon_g \sigma\left(T_w^4 - T_g^4\right) + (0.844)\left[(T_w - T_{gi}) + \left(\frac{(P_w - P_{gi})(T_w + 273)}{2.689 \times 10^5 - P_w}\right)\right]^{1/3}(T_w - T_{gi}) \times (0.016273) h_{cw}\,(P_w - P_g) = A_r \varepsilon_g \sigma\left(T_g^4 - T_{sky}^4\right) + h_w (T_g - T_a) \quad (29)$$

Kumar et al. developed a simplified form of empirical equation for hybrid (PV/T) active solar still to estimate the glass temperature. The linear and non-linear equation for internal HTCs external HTCs respectively has been developed on the basis of experimental performance for 0.05 m water depth to obtain the more close results (Eq. (29). The developed equations are expressed as

$$h_{1w} = 2991.684 - 19.8\,T_w + 0.033 T_w^2 \quad (30)$$

$$h_{rg} = 0.141\,T_a - 36.026 \quad (31)$$

Hence, the glass cover temperature of the still can be written as

$$T_g = \frac{\left(2991.684 - 19.8\,T_w + 0.033 T_w^2\right) T_w + A_r h_w T_w + A_r (0.141\,T_a - 36.026) T_s}{\left(2991.684 - 19.8\,T_w + 0.033 T_w^2\right) + A_r h_w + A_r (0.141\,T_a - 36.026)} \quad (32)$$

It has been observed that the enhancement in wind HTC decreases the glass temperature and it increases with enhancement in temperature of water (Fig. 13(a)). The estimated value of glass temperature has been used further to evaluate the various heat transfer coefficients. The difference among the internal and external HTCs differs with water temperature enhancement (Fig. 13(b)). The effect of wind HTC is minimal at lower water temperature (~30 °C) which is due to low temperature difference between glass surface and ambient. These evaluated internal HTCs are further used to estimate the energy fractions in the still cavity. The relative influence of convective, radiative and evaporative energy fractions are shown in Fig. 14. It has been observed that evaporative heat transfer mode dominates over the convective and radiative heat transfer modes. The distillate output and system efficiency is higher for higher evaporative energy fraction. The obtained experimental results are close to the developed model and numerical solutions (Fig. 14(b)).

3.3. Characteristic equation of a hybrid (PV/T) active solar still [62]

As explained earlier (Section 2.2), the concept of efficiency is real important for the design and improvement in the solar still performance. Characteristic equation can be used for further modifications in the existing design in terms of design, operating and climatic factors etc.

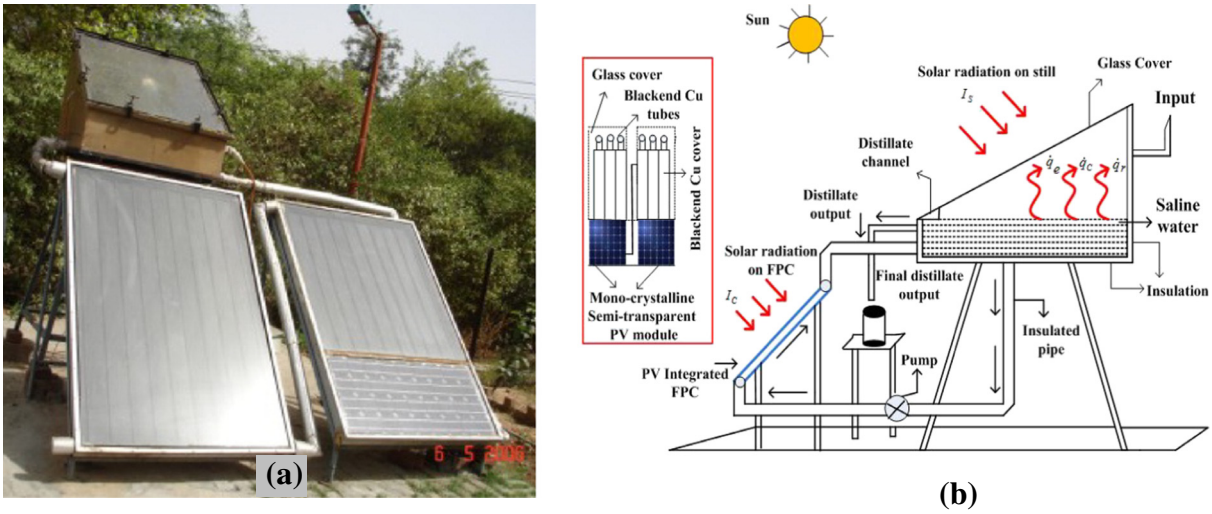

Fig. 11. (a) Experimental setup [60] and (b) schematic view of an integrated hybrid (PV/T) active solar still.

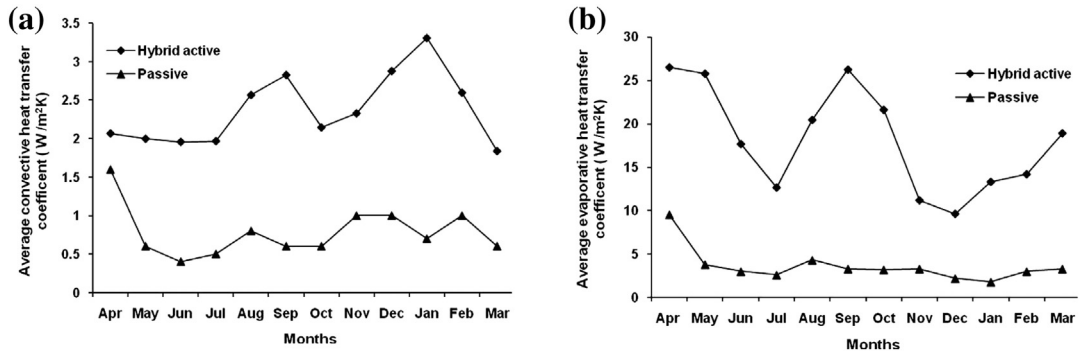

Fig. 12. Comparative monthly variation of average (a) convective (b) evaporative heat transfer coefficient in passive and hybrid active solar still at 0.05 m water depth [60].

Dev and Tiwari [62] established the characteristic equation of hybrid (PVT) active solar still on the basis of annual experimental observations. The experimental setup was installed at the Solar Energy Park, Indian Institute of Technology, New Delhi (Fig. 11(a)). Analytical expression has been derived for instantaneous gain and loss efficiency of the system.

The energy balances for different components of the system are given as

(i) Glass cover

$$\alpha_g I_S(t) + h_{1w}(T_w - T_{gi}) = h_{1g}(T_{gi} - T_a) \tag{33}$$

(ii) Water mass

$$M_w C_w \frac{dT_w}{dt} + h_{1w}(T_w - T_{gi}) = \alpha_w I_S(t) + h_{ba}(T_b - T_w) + \dot{q}_u \tag{34}$$

where, $\dot{q}_u = [A_m F_{Rm} h_{p2}(\alpha\tau)_{m,eff}\left(1 - \frac{A_c F_{Rc} U_{L,c}}{\dot{m}}{}_f C_f\right) + A_c F_{Rc}(\alpha\tau)_{c,eff}]I_c(t) - [A_m F_{Rm} U_{L,m}\left(1 - \frac{A_c F_{Rc} U_{L,c}}{\dot{m}_f C_f}\right) + A_m F_{Rc} U_{L,c}](T_{fi} - T_a)$

The unknowns in above equation are given in Appendix A [62].

(iii) Basin liner

$$\alpha_b I_S(t) = h_{ba}(T_b - T_w) + h_b(T_b - T_a) \tag{35}$$

Solving above equations, temperature of basin water can be expressed as

$$T_w = \frac{\overline{f'(t)}}{a}\left[1 - e^{-a\Delta t}\right] + T_{w0}\, e^{-a\Delta t} \tag{36}$$

Instantaneous thermal efficiency (gain) can be expressed as

$$\eta_i = \frac{\dot{q}_{ew}}{(A.I(t))_{eff}} = \left(\frac{h_{ew} h_{1g}}{h_{1w} + h_{1g}}\right)\left(\frac{(T_w - T_a)}{I_s(t) + \eta_c A_c' I_c(t)}\right) \tag{37}$$

Case 1. : $(I_s(t) = I_c(t))$

$$\eta_i = F'\left[(\alpha\tau)_{eff1}\left(1 - e^{-a\Delta t}\right) + (U)_{eff1} e^{-a\Delta t}\left(\frac{T_w - T_a}{I_s(t)}\right)\right] \tag{38}$$

Case 2. : $(I_s(t) \neq I_c(t))$

$$\eta_i = F''\left[(\alpha\tau)_{eff2}\left(1 - e^{-a\Delta t}\right) + (U)_{eff2} e^{-a\Delta t}\left(\frac{T_w - T_a}{I_s(t)}\right)\right] \tag{39}$$

$$\eta_i = m_1\left(\frac{T_w - T_a}{I(t)}\right) + C_1 \text{ (linear characteristic equation)} \tag{40}$$

where, $m_1 = F''(U)_{eff2} e^{-a\Delta t}$; and $C_1 = F''(\alpha\tau)_{eff2}(1 - e^{-a\Delta t})$ are the regression coefficients. Similarly, the instantaneous thermal loss efficiency can be expressed as

$$\eta_{iL} = \left[(\alpha\tau)_{EFF} - U_L''\frac{(T_w - T_a)}{I(t)}\right] \text{ Or } \eta_{iL} = m_2\left(\frac{T_w - T_a}{I(t)}\right) + C_2 \text{ (linear characteristic equation)} \tag{41}$$

where, $m_2 = -U_L'$; and $C_2 = (\alpha\tau)_{EFF}$.

The unknowns in Eq. (39) and Eq. (41) are given in Appendix A [62].

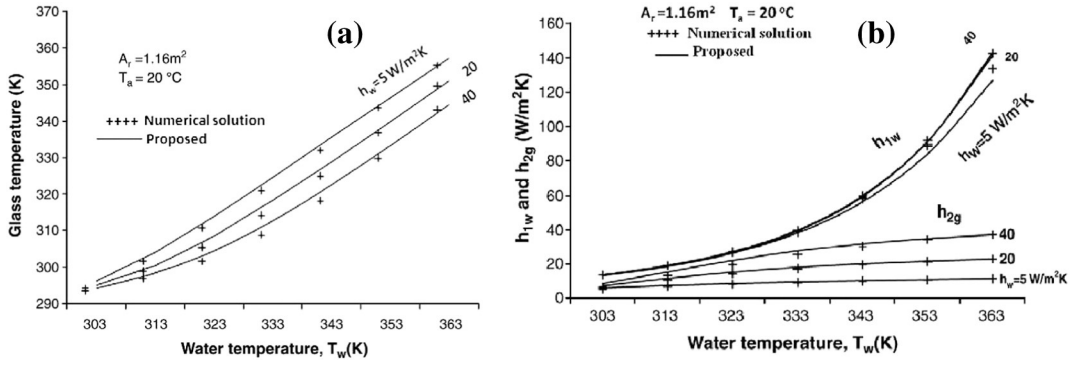

Fig. 13. Variation of (a) glass temperature and (b) total internal (h_{1w}) and external (h_{2g}) HTCs of hybrid active solar still with basin water temperature.

Please cite this article as: G.N. Tiwari, L. Sahota, Review on the energy and economic efficiencies of passive and active solar distillation systems, Desalination (2016), http://dx.doi.org/10.1016/j.desal.2016.08.023

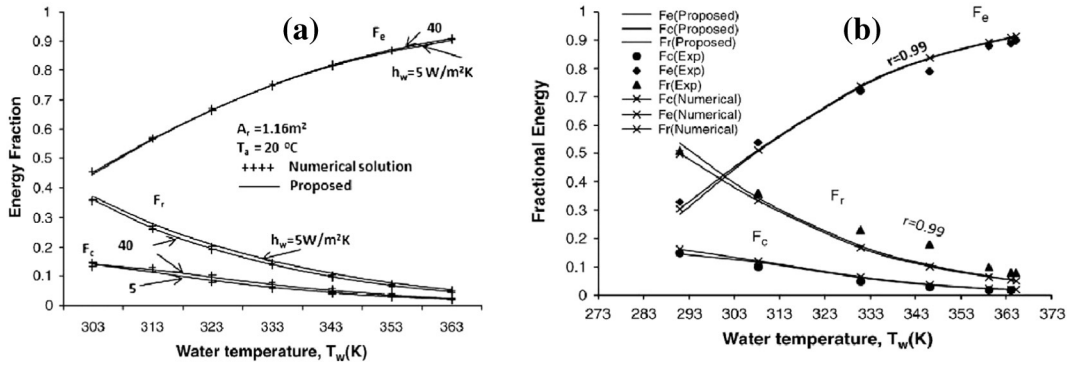

Fig. 14. (a) Relative influence of energy fractions (evaporative, convective and radiative) using proposed models and numerical solutions and (b) experimental validation.

Quantitatively, the constants m_1 and m_2 (method-1) represent the overall HTCs. The higher input radiation has been retrieved by the system during the months of April, September and March which gives the higher value of m_1. On the other hand, m_1 remains low for the months June and July irrespective of higher solar intensity and ambient temperature. Furthermore, it has been observed that the extreme values of the gain and loss efficiencies are similar for the linear characteristic equations while these are different in case of non-liner characteristic equations (Fig. 15(a) and (b)).

In similar manner to the characteristic equation of FPC, Dev and Tiwari further made an attempt to develop the characteristic equation using matrix method (method-2) for the solar still. Consequently, due to lower root mean square (RMS) percentage error, it is recommended to use the nonlinear characteristic equation obtained by method-1 for the thermal testing of a hybrid (PV-T) active solar still. On the annual basis, it has been found that the non-linear characteristic equations estimated by method-1 are considered to be used for the thermal testing instead of non-linear characteristic equations evaluated from method-2.

3.4. Active double slope solar still (DSSS) under natural circulation mode [63]

Dwivedi and Tiwari [63] developed thermal modeling of active double slope solar still (DSSS) under the natural circulation mode (Fig. 16(a) and (b)). They experimentally validated the developed thermal model and furthermore evaluated the energy and exergy efficiency of the system for fixed (0.03 m) water depth. The analysis has been carried out for a typical day of the month March for the composite climate of Ghaziabad (28°40′N, 77°25′E), U.P., India.

Following Dwivedi and Tiwari [63], the energy balance of different components of the system are given as

(i) Glass cover (East side)

$$\alpha_g I_E + h_{1wE}(T_w - T_{giE}) - U_{EW}(T_{giE} - T_{giW}) = h_{aE}(T_{goE} - T_a) \tag{43}$$

(ii) Glass cover (West side)

$$\alpha_g I_W + h_{1wW}(T_w - T_{ciW}) - U_{EW}(T_{giE} - T_{giW}) = h_{aW}(T_{goW} - T_a) \tag{44}$$

(iii) Water mass

$$M_w C_w \frac{dT_w}{dt} = \alpha_w(I_E + I_W) + 2h_{bw}(T_b - T_w) - h_{1wE}(T_w - T_{giE}) - h_{1wW}(T_w - T_{giW}) + \dot{Q}_u \tag{45}$$

where, $\dot{Q}_u = A_c F'[(\alpha\tau)I_c(t)] - U_L(T_w - T_a)$

(iv) Basin liner

$$\alpha_b(I_E + I_W) = 2h_{bw}(T_b - T_w) + 2h_{ba}(T_b - T_a) \tag{46}$$

Solving above equations, temperature of basin water can be expressed as

$$T_w = \frac{\overline{f'(t)}}{a}\left[1 - e^{-a\Delta t}\right] + T_{w0}\, e^{-a\Delta t} \tag{47}$$

The outer and inner glass temperatures; and yield for the east and west side can be expressed as

$$T_{giE} = \frac{A_1 + A_2 T_w}{p};\ T_{giW} = \frac{B_1 + B_2 T_w}{p};\ T_{goE} = \frac{\left(\frac{K_g}{L_g}\right)T_{giE} + h_{aE}T_a}{\frac{K_g}{L_g} + h_{aE}};\ T_{coW} = \frac{\left(\frac{K_g}{L_g}\right)T_{giW} + h_{aW}T_a}{\frac{K_g}{L_g} + h_{aW}}; \tag{48}$$

The unknowns in above equations are given in Appendix A [63].

The overall thermal energy (η_{EN}) and exergy (η_{EX}) efficiency of DSSS system can be written as

$$\text{(a) Passive}: \eta_{EN} = \frac{\sum \dot{m}_{ew} \times L}{\sum (I(t))_t \times A_s \times 3600};\ \text{and}\ \eta_{EX} = \frac{\left[A_g \times h_{ew} \times (T_w - T_{giE}) \times \left(1 - \frac{T_a + 273}{T_w + 273}\right)\right]}{A_g \times I(t) \times \left[1 - \frac{4}{3}\left(\frac{T_a + 273}{T_s}\right) + \frac{1}{3}\left(\frac{T_a + 273}{T_s}\right)^4\right]} \tag{49}$$

$$\text{(b) Active}: \eta_{EN} = \frac{\sum \dot{m}_{ew} \times L}{\sum \left[(I(t))_s \times A_g \times 3600\right] + \sum \left[(I(t))_c \times A_c \times 3600\right]} \tag{50}$$

$$\eta_{EX} = \frac{\left[A_g \times h_{ew} \times (T_w - T_{giE}) \times \left(1 - \frac{T_a + 273}{T_w + 273}\right)\right]}{A_g \times I(t) \times \left[1 - \frac{4}{3}\left(\frac{T_a + 273}{T_s}\right) + \frac{1}{3}\left(\frac{T_a + 273}{T_s}\right)^4 + \dot{Q}_u\left(1 - \frac{T_a + 273}{T_w + 273}\right)\right]} \tag{51}$$

It has been perceived that the water temperature of active DSSS is significantly higher around 10 °C than the passive solar still (Fig. 17(a)) which happens due to additional thermal energy transferred by the FPC to the still basin. Fig. 17(b) and (c) shows that the maxima of east side is lagging with the maxima of west side of the glass cover which happens due to maximum solar intensity at east and west side of the glass cover at 1 pm and 2 pm respectively. The hourly yield obtained from the west side is higher in comparison to the east side during the morning hours (Fig. 17(d)). It occurs due to the cooler west side cover in the morning hours in comparison to the

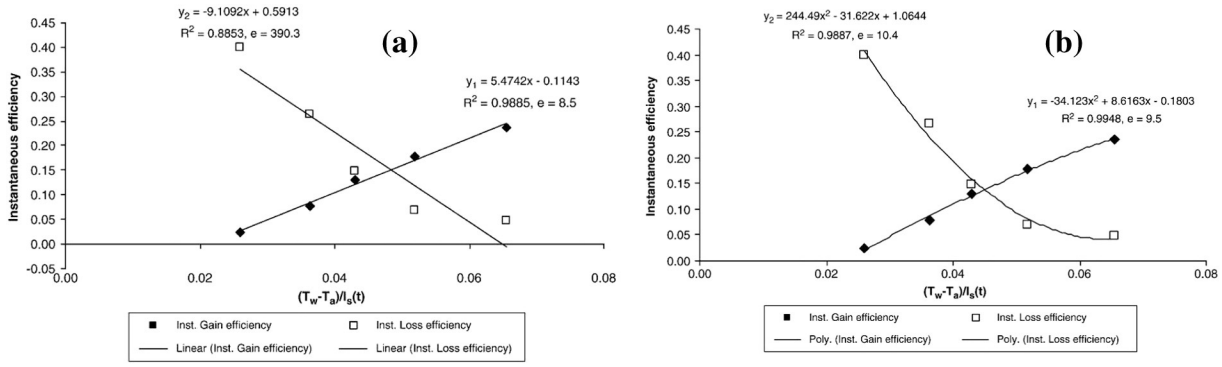

Fig. 15. (a) Linear and (b) non-linear characteristic curves of hybrid (PVT) active solar still for water depth 0.05 m on annual average basis.

east condensing cover. The daily yield of active DSSS under natural mode (2.79 kg/m^2) for a typical day of the month March is found to be higher than the passive DSSS (1.838 kg/m^2). The thermal energy efficiency of passive solar still (0–23.9%) is always found to be higher than the thermal efficiency of active solar still (0–17.9%). The overall average thermal energy and exergy efficiencies of FPC coupled with DSSS are 10.34% and 1.16%, respectively.

In case of N-PVT-CPC coupled with solar distillation system reported by Singh et al. [105], the double slope performs better than single slope PVT-CPC active solar distillation system on the basis of yield if the basin water depth is lower than 0.19*m* and vice-versa. It is credited to the fact that the water temperature is higher at its lower depth in basin; and moderate solar intensity exists for a longer period in the case of double slope PVT-CPC active solar distillation system. Consequently, a moderate temperature difference of basin water and glass exists for a longer period in the case of double slope PVT-CPC active solar distillation system. However, in the case of single slope PVT-CPC active solar distillation system, this difference is higher but it exists for a shorter period. Hence, higher daily yield is obtained for double slope PVT-CPC active solar distillation system at lower basin water depth. In the day time, the rise in basin water temperature is lesser at higher water depth, while the sensible heat of basin water mass will be higher for single slope PVT-CPC active solar distillation system. Therefore, daily yield for single slope is higher than double slope PVT-CPC active solar distillation system at higher depth of water. The daily yield increases with the increase in number of collectors due to higher heat gain as expected.

The outlet temperature of Nth PVT-CPC collector becomes more than 100 °C on increasing the number of collectors greater than seven for the proposed system. In such cases, another fluid having higher boiling point (salts) can be used along with heat exchanger so that heat gain can be transferred to the water in basin.

3.5. Optimization of number of collectors of hybrid (PVT) active solar still [64]

Gaur and Tiwari [64] made efforts to optimize the number of series connected collectors of photovoltaic thermal (PVT) hybrid active solar still (Fig. 18). The analysis has been carried out on the basis of energy and exergy for the month May of New Delhi climatic conditions. The present system consists of hybrid FPC and a conventional solar still (Area 1 m^2; glass angle 30°). The hybrid FPC is partially covered by the semi-transparent PV module (37 W_P) to run the D.C. pump. The outlet of Nth PVT partially covered flat plate collector is connected to the conventional SSSS system and the rate of useful thermal energy $\dot{Q}_{uth,N}$ is added to the thermal energy of water mass in the still. The losses have been minimized by insulating the connecting pipes. Energy

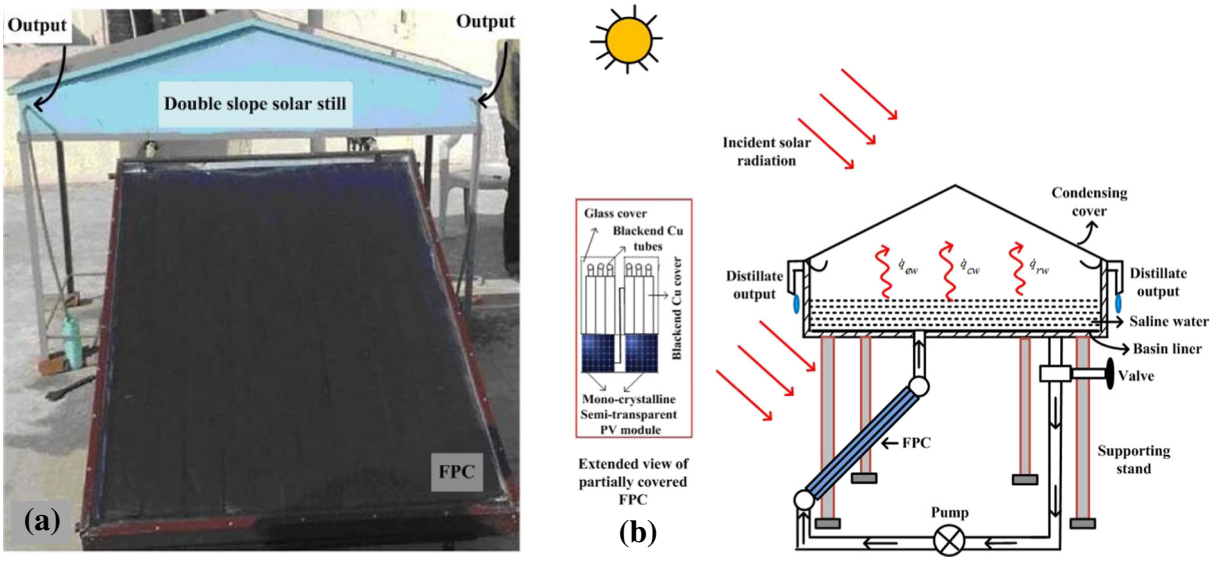

Fig. 16. (a) Experimental setup and (b) schematic view of active double slope solar still.

Please cite this article as: G.N. Tiwari, L. Sahota, Review on the energy and economic efficiencies of passive and active solar distillation systems, Desalination (2016), http://dx.doi.org/10.1016/j.desal.2016.08.023

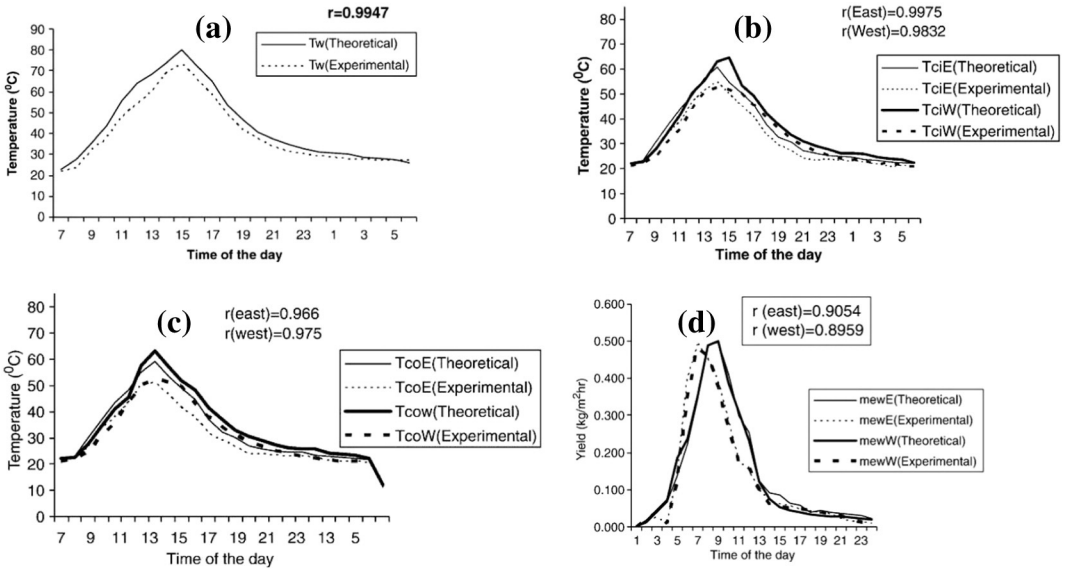

Fig. 17. Hourly variation of (a) water temperature, (b) temperature of inner surface of glass cover (east and west side), (c) temperature of outer surface of the glass cover (east and west side), and (d) yield for atypical day of the month March for 0.03 m water depth of active double slope solar still.

balance equation of different components of N-PVT partially covered FPC connected in series integrated to SSSS are given as follows;

(i) Inner glass cover

$$\alpha_g I(t)A_g + h_{1w}(T_w - T_{gi})A_g = \frac{K_g}{L_g}(T_{gi} - T_{go})A_g \tag{52}$$

(ii) Outer glass cover

$$\frac{K_g}{L_g}(T_{gi} - T_{go})A_g = h_{1g}(T_{go} - T_a)A_g \tag{53}$$

(iii) Water mass

$$\alpha_w I(t)A_b + h_{bw}(T_b - T_w)A_b + \dot{Q}_{uth,N} = M_w C_w \frac{dT_w}{dt} + h_{1w}(T_w - T_{gi})A_b \tag{54}$$

(iv) Basin liner

$$\alpha_b I(t)A_b = h_{bw}(T_b - T_w)A_b = h_{ba}(T_b - T_a)(A_b + A_{sd}) \tag{55}$$

Following Dubey and Tiwari [65], the rate of useful thermal energy from partially covered N-photovoltaic thermal flat plate collectors (PVT-FPC) connected in series is

$$\dot{Q}_{uth,N} = N(A_c + A_m)\left[(\alpha\tau)_{eff,N} I_c(t) - U_{L,N}(T_{fi} - T_a)\right] \tag{56}$$

Therefore, solving Eq. (54), one can get;

$$\frac{dT_w}{dt} + \left[\frac{U + N(A_c + A_m)U_{L,N}}{M_w C_w}\right]T_w = \frac{\left[\alpha_{eff} I(t) + N(A_c + A_m)(\alpha\tau)_{eff,N} I_c(t) + (U + N(A_c + A_m)U_{L,N})\right]}{M_w C_w}$$

$$\frac{dT_w}{dt} + aT_w = f(t) \tag{57}$$

All the unknowns in above equation are given in Appendix A [64]. Solving Eq. (57), the temperature of water can expressed as

$$T_w = \frac{\overline{f(t)}}{a}\left[1 - e^{-a\Delta t}\right] + T_{w0}\, e^{-a\Delta t} \tag{58}$$

Exergy of the active system can be expressed as

$$\sum \dot{E}_{X,in} - \sum \dot{E}_{X,out} = \sum \dot{E}_{X,dest} \tag{59}$$

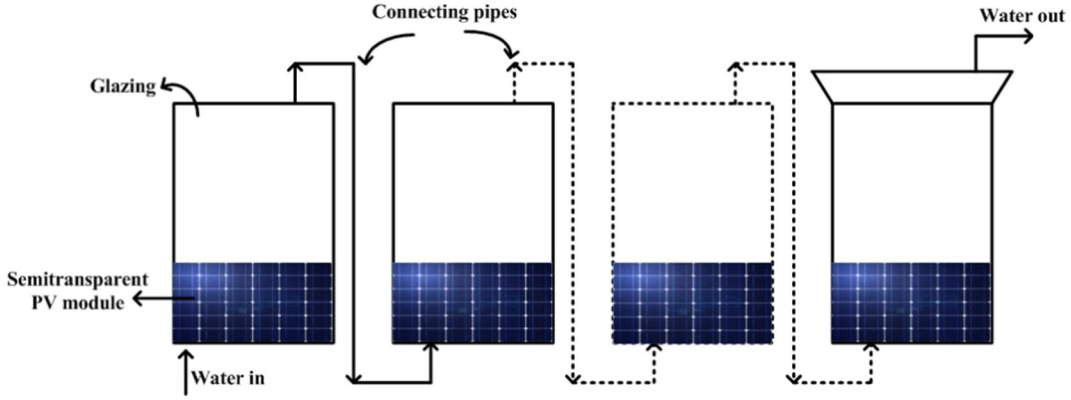

Fig. 18. Illustrative view of photovoltaic thermal (PVT) N-collectors connected in series.

Please cite this article as: G.N. Tiwari, L. Sahota, Review on the energy and economic efficiencies of passive and active solar distillation systems, Desalination (2016), http://dx.doi.org/10.1016/j.desal.2016.08.023

where, $\sum \dot{E}_{X,out} = \times A_b \dot{q}_{ew}(1-\frac{T_a+273}{T_w+273})$; and $\sum \dot{E}_{X,in} = \dot{E}_{X,in}(solarstill) + \dot{E}_{X,in}(PVT/FPC)$

$$\dot{E}_{X,in}[((PV/T)FPC)] = I(t)(A_c + A_m)\sum\left[1-\frac{4}{3}\left(\frac{T_a+273}{T_s}\right)+\frac{1}{3}\left(\frac{T_a+273}{T_s}\right)^4\right] \quad (60)$$

$$\dot{E}_{X,in}[(Solarstill)] = I_s(t)A_b\sum\left[1-\frac{4}{3}\left(\frac{T_a+273}{T_s}\right)+\frac{1}{3}\left(\frac{T_a+273}{T_s}\right)^4\right] \quad (61)$$

The overall thermal energy (η_{EN}) and exergy efficiency (η_{EX}) of the system can be expressed as

$$\eta_{EN} = \frac{\sum \dot{m}_{ew} \times L}{[(A_b \sum I_s(t)) + +(N \times A \times \sum I'(t))] \times \Delta t} \quad (62)$$

$$\eta_{EX} = 1-\frac{\left[M_w C_w \times (A_b + A_g) \times (T_w - T_{gi}) \times \left(1-\frac{T_a+273}{T_w+273}\right)\right]}{\dot{E}_{X,in}(solarstill) + \dot{E}_{X,in}(PVT/FPC)} \quad (63)$$

The daily efficiency decreases gradually on increasing the number of PVT collectors while the daily exergy efficiency first increases up to two collectors then starts decreasing after the two number of PVT collectors (Fig. 19(a)). The daily yield and daily exergy efficiency of the system reduces approximately by 46% on increasing the basin water mass from 50 kg to 200 kg (Fig. 19(b)). Furthermore, the increase in number of PVT collectors' (upto $N=2$) enhances the basin water temperature which intern increases the daily exergy (Fig. 19(c)). The variation of daily exergy efficiency with number of PVT collectors for different basin water masses has been depicted in Fig. 19(d). It is found that the daily exergy efficiency is maximum (69%) for two PVT collectors and lower basin water mass (50 kg) and it decreases on increasing the water mass from 50 kg to 200 kg. On the basis of exergy efficiency, the combination of four PVT collectors ($N=4$) and 50 kg basin water mass gives the maximum yield.

3.6. Study of a hybrid (PVT) double slope active solar still [66]

Singh et al. [66] designed a modified photovoltaic thermal active double slope solar still (DSSS) and fabricated for remote locations. The experiment was performed under the natural and forced circulation mode (series and parallel) for the climatic conditions of Ghaziabad, India in the month of October. They made an attempt to study the system performance (experimentally) to get the best configuration (Fig. 20(a)) in natural and forced circulation modes (series (Fig. 20(b)) and parallel (Fig. 20(c)).

The constructed system mainly comprises of three components viz. DSSS (2×1 m^2, glass inclination 15°), PVT-FPCs and DC water pump. The still is kept in east-west orientation to retrieve the maximum solar radiation as explained earlier. The FPCs ($N=2$) each of area 2 m^2 are coupled to the still basin via insulated pipes (minimum losses). A glass to glass photovoltaic (PV) module (0.55×1.25 m^2) of 36 cells has been integrated at the collector's bottom side. The working mechanism has been explained earlier in Section 3.

The energy matrices have been evaluated for the present system as given below;

(a) Energy analysis: The daily energy efficiency the system can be expressed as

$$\eta_{EN} = \frac{\sum \dot{m}_{ew} \times L}{\sum\left[(I_s(t))_E \times A_{gE} + (I_s(t))_W \times A_{gW}\right] \times 3600 + \sum\left[(I(t))_c \times (A_c + A_m) \times 3600\right]} \times 100 \quad (64)$$

(b) Exergy analysis: The general exergetic analysis for solar still can be given as

$\sum \dot{E}_{X,in} - \sum \dot{E}_{X,out} = \sum \dot{E}_{X,dest}$ Or $\sum \dot{E}_{X,sun} - (\sum \dot{E}_{X,evp} - \sum \dot{E}_{X,work}) = \sum \dot{E}_{X,dest}$ where,

$$\begin{aligned}\dot{E}_{X,sun} &= \left\{\left[(I_s(t))_E \times A_{gE} + (I_s(t))_W \times A_{gW}\right] + \left[(I(t))_c \times (A_c + A_m)\right]\right\} \\ &\times \left[1-\frac{4}{3}\left(\frac{T_a+273}{T_s}\right)+\frac{1}{3}\left(\frac{T_a+273}{T_s}\right)^4\right] \\ &= \left[(I_s(t))_E \times A_{gE} + (I_s(t))_W \times A_{gW}\right] + \left[(I(t))_c \times (A_c + A_m)\right] \\ &\times 0.933\end{aligned} \quad (65)$$

The daily exergy output from the solar still is given as

$$\dot{E}_{X,evap} = \sum\left(1-\frac{T_a+273}{T_w+273}\right)m_{ew}L \quad (66)$$

The exergetic efficiency can be evaluated as;

$$\eta_{EX} = \frac{\dot{E}_{X,evap}}{\dot{E}_{X,in}} = \frac{\dot{E}_{X,evap}}{\dot{E}_{X,sun}(solarstill) + \dot{E}_{X,sun}(FPC) + \dot{E}_{X,sun}(PV)} \quad (67)$$

(c) Energy payback time (EPBT) [66]:

$$EPBT = \frac{Emboidedenergy}{Annualoutputenergyfromthesystem} \quad (68)$$

It has been observed that the parallel forced mode configuration gives enhanced values of the energy (maximum 32%) and exergy (maximum 2.3%) efficiencies for most of the time (Fig. 21(a)). The daily energy efficiency obtained with parallel forced mode configuration (17.4%) is found to be higher in comparison to the series (16.4%) and natural circulation modes (16.3%). It has been concluded that the parallel forced mode gives the better results such that it can be opted to operate among the others. The annual yield obtained from the system is 1616 kg, 1777 kg and 1939 kg for 250, 275 and 300 number of days respectively (Fig. 21(b)). The estimated EPBT is found to be three years for the passive SSSS which is significantly lower (30%) than the hybrid (PVT) SSSS system.

3.7. Economic analyses of partially covered PVT-FPC active solar still [67]

Enviroeconomic analysis is based upon the cost of CO_2 emission and propels to utilize the non-conventional sources of energy such that renewable technology which does not emit carbon to the environment. On the other hand, an exergoeconomic method is a combination of exergy analysis with the cost analysis to improve the performance of renewable energy systems. It enables the designers to find an alternative ways or techniques to improve the system performance from the cost point of view. Tiwari et al. [67] presented an exergoeconomic and enviroeconomic analyses of partially covered photovoltaic thermal (PVT) flat plate collector (FPC) coupled with conventional solar still (Fig. 11) for the composite climate of New Delhi, India. They experimentally estimated the hourly thermal, exergy, electrical, overall exergy and overall thermal efficiency and compared the obtained results with the results proposed by earlier researchers.

The hourly overall exergy efficiency of hybrid (PV/T) active solar still can be expressed as

$$\eta_{hourly,overall\ EX} = \frac{h_{ew}\left[(T_w - T_{gi}) - (T_a + 273) \times \left(\frac{T_w+273}{T_{gi}+273}\right)\right] + [FF \times V_{oc} \times I_{sc} - V_L \times I_L]}{[(A_c + A_m) \times I_c(t) + A_{still} \times I_s(t)] \times 0.99} \times 100 \quad (69)$$

Please cite this article as: G.N. Tiwari, L. Sahota, Review on the energy and economic efficiencies of passive and active solar distillation systems, Desalination (2016), http://dx.doi.org/10.1016/j.desal.2016.08.023

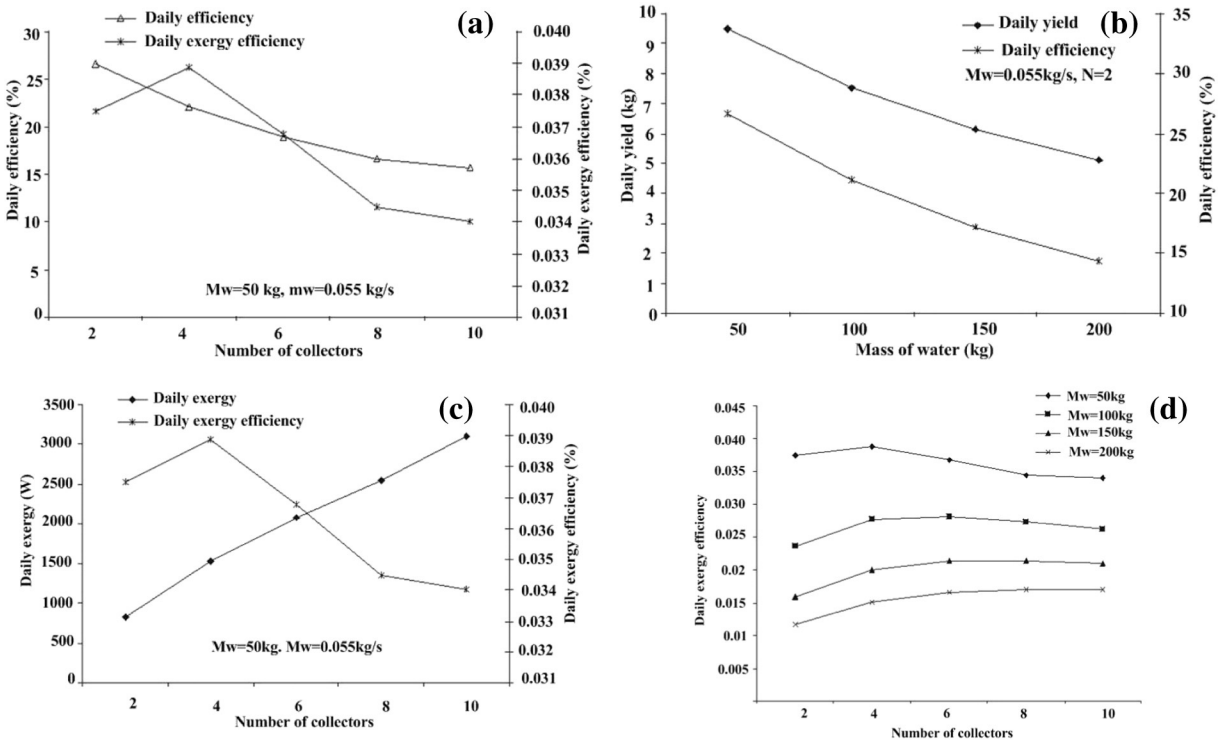

Fig. 19. Variation of (a) daily efficiency and daily exergy efficiency with number of collectors for 0.055 kg/s mass flow rate and 50 kg basin water mass, (b) daily yield and daily efficiency with water mass in the still for 0.055 kg/s mass flow rate and $N=2$ collectors, (c) daily exergy and daily exergy efficiency with number of collectors for 0.055 kg/s mass flow rate and 50 kg basin water mass, and (d) daily exergy efficiency with number of collectors at different basin water masses.

Hourly overall thermal energy efficiency of the system can be expressed as

$$\eta_{hourly,overall\ EN} = \frac{\dot{m}_{ew} \times L \times 100}{((I(t))_s \times A_{stil} + (I(t))_c \times A_c) \times 3600} + \frac{FF \times V_{oc} \times I_{sc}}{0.38 \times A_m \times I_c} \times 100 \quad (70)$$

This analysis has been performed on the basis of price of emitted CO_2. The amount of CO_2 emitted per kWh is approximately 0.960 kg [68]. The amount of CO_2 emitted per annum [68] is given by,

$$\varphi_{CO_2} = \frac{\psi_{CO_2} \times overallexergy}{1000} \quad (71)$$

Here, φ_{CO_2} = CO_2 emitted per annum from hybrid PVT array in ton/annum and ψ_{CO_2} = average CO_2 equivalent intensity for electricity generation from coal (2.0 kg CO_2/kWh. The net CO_2 emission evaluated for the life span of 30 years is found to be 13.02 tons. The international carbon price (z CO_2) is 14.5 dollar per ton of CO_2 [69]. The environmental cost Z CO_2 is given by Rajoria et al. [70] as

$$Z\ CO_2 = z\ CO_2 \times \varphi_{CO_2} \quad (72)$$

Hence, environmental cost which is also called enviroeconomic parameter comes out to be 6.29$ per annum and for the life span of 10 years, it is estimated as 60.29$.

Further, the exergoeconomic analysis of the system has been also carried out by Tiwari et al. The exeroeconomic parameter is given as

$$R_{ex} = \frac{L_{ex,annual}}{UAC} \quad (73)$$

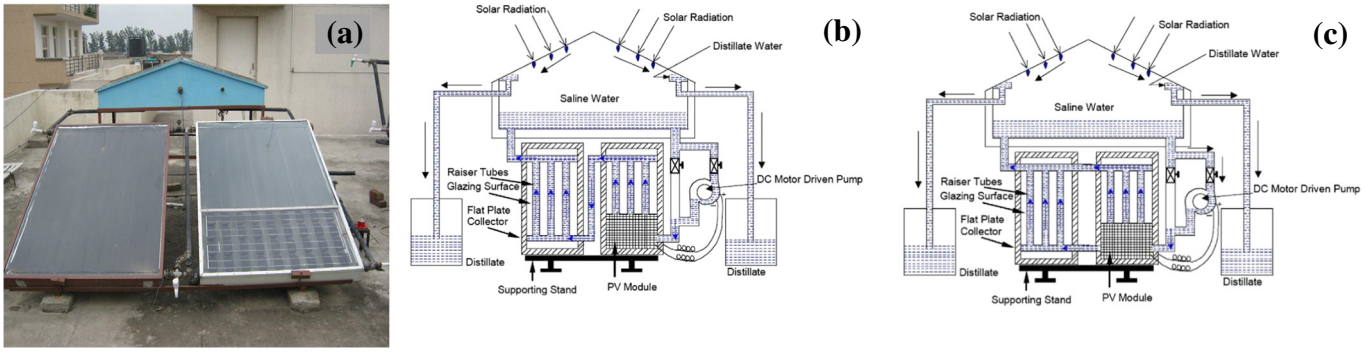

Fig. 20. (a) experimental setup of active double slope solar still (DSSS) in forced circulation mode coupled with FPCs. Schematic view of active DSSS in forced circulation mode coupled with FPCs connected in (b) series and (c) parallel.

Please cite this article as: G.N. Tiwari, L. Sahota, Review on the energy and economic efficiencies of passive and active solar distillation systems, Desalination (2016), http://dx.doi.org/10.1016/j.desal.2016.08.023

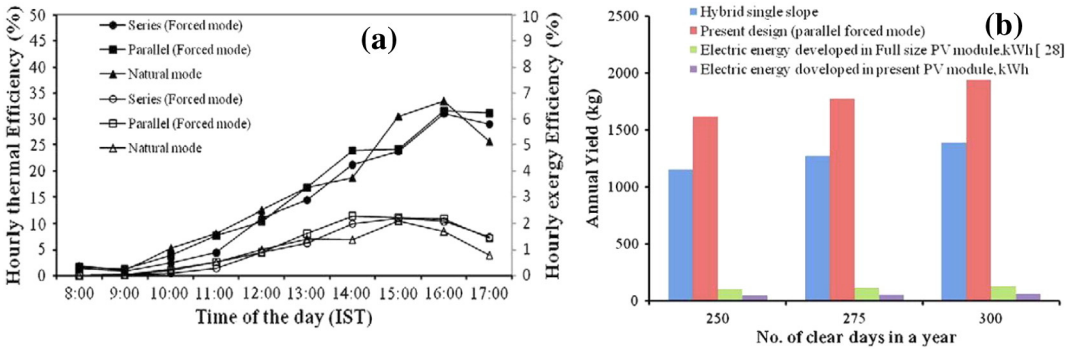

Fig. 21. (a) Hourly variation of thermal energy and exergy efficiency of hybrid double slope active solar still in different operational modes, and (b) comparative estimated annual yield and electric energy obtained from present design (parallel forced mode) for different numbers of clear days in a year.

where, the exergoeconomic loss rate (L_{ex}) can be expressed as [71],

$$L_{ex} = (h_{cw} + h_{rw})\left[(T_w - T_{gi}) - (T_a + 273) \times \left(\frac{T_w + 273}{T_{gi} + 273}\right)\right] + (M_w C_w)\left[(T_{wf} - T_{wi}) - (T_a + 273) \times \left(\frac{T_{wf} + 273}{T_{gwi} + 273}\right)\right] \quad (74)$$

Following Tiwari and Ghosh [72],

$$UAC = P_s F_{CR,i,n}(1 + M_s) + R_{r,5} F_{CR,i,n} + R_{r,10} F_{CR,i,n} + R_{r,15} F_{CR,i,n} \ldots\ldots\ldots\ldots - S_s F_{SR,i,n} \quad (75)$$

where, P_s, S_s and M_s are the net present value, salvage value and maintenance cost of the system. The capital recovery factor ($F_{CR,i,n}$) and sinking fund factor ($F_{SR,i,n}$) are given as

$$F_{CR,i,n} = \frac{i(1+i)^n}{(1+i)-1}; \text{and } F_{SR,i,n} = \frac{i}{(1+i)^{n-1}}$$

Considering the replacement time of DC pump as 10 years, the net present cost (P_s) for 30 years life span of the active solar still is given by Tiwari [73],

$$P_s = P + P_P + \frac{P_p}{(1+i)^{10}} + \frac{P_p}{(1+i)^{20}} \quad (76)$$

where, P_P is the pump cost and P is the initial cost of the active system.

The theoretically estimated results of the system (proposed model) have been compared with the experimental results of the present model (model 1) and the earlier results given by Kumar and Tiwari [74] (model 2). The monthly variation of exergy gain exergy loss has been also presented in Fig. 22(a) and (b) respectively. The exergy gain has been found maximum during the month of September and June due to availability of maximum solar radiation. On the other hand, the exergy loss has been observed maximum in the month of October and March. The proposed model gives the higher values of daily electrical exergy efficiency, the daily overall exergy efficiency and the daily overall thermal efficiency in comparison to the other two models. Later, Singh et al. [75] estimated the thermal, exergy and overall thermal efficiency of the partially covered two hybrid PVT -FPC solar still and compared the consequences with the theoretical results. In case of hybrid active N-PVT-FPC, single slope performs better than double slope active solar still integrated with N-PVT-FPC on the basis of yield if depth is >0.15 m and vice versa if depth is less than 0.15 m. Whereas, double slope active solar still performs better than single slope active solar still integrated with N-PVT-FPC on the basis of exergoeconomic parameter, enviroeconomic parameter, energy matrices and productivity at 0.14 m water depth for same basin area ($N = 11$, $\dot{m}_f = 0.03$ kg/s).

3.8. Life cycle cost analysis of single slope hybrid (PVT) active solar still [76]

The energy matrices (EPBT, EPF, and LCCE) are important for renewable technologies as their use makes no sense if the energy used in their manufacture is more than they can produce in their life-time. The energy payback time (EPBT) is always be one of the criteria used for comparing the viability of one renewable technology against another. It defines the time period needed to recuperate the total energy exhausted in the material preparation for the system fabrication. It depends on the embodied energy and the annual energy output obtained from the system. The life cycle cost of the system help the designers to fabricate the system in cost effective manner.

On the basis of annual performance, Kumar and Tiwari [76] studied the life cycle cost analysis of the passive single slope and hybrid photovoltaic (PVT) active solar stills. Experiments on both the systems have been performed in the solar energy park of I.I.T New Delhi (India) for three different basin water depths (0.05 m, 0.10 m, and 0.15 m) for a typical day. They estimated the effect of various parameters viz. interest rate, system's life span, maintenance cost, PBT and EPBT considering the initial investment and salvage value of the system. Kumar and Tiwari performed the economic analysis of the systems as follow:

The net present cost (*Ps*) for 30 year life span of hybrid (PVT) active solar still can be expressed as;

$$P_s = P + \frac{P_p}{(1+i)^{10}} + \frac{P_p}{(1+i)^{20}} + \frac{(P_{FPC})_{total}}{(1+i)^{15}} \quad (77)$$

Uniform annual cost can be obtained from Eq. (74).

The net effective annualized cost of the active system can be expressed as

$$(UA)_{Net} = UA + S_{p,elect}(P_m - P_u) \quad (78)$$

The cost of distilled water per kg,

$$CPK = \frac{(UA)_{Net}}{M_{yield}} \quad (79)$$

Cost payback period (n_p) can be expressed as;

$$n_p = \frac{\ln\left[\frac{CF}{CF - i P_s}\right]}{\ln(1+i) = \ln\left[\frac{CF}{CF - i \times (\text{Cash flow} \times F_{RP,i,n})}\right]} \quad (80)$$

From the analysis, it has been perceived that the hybrid (PVT) active solar still gives higher yield in comparison to the passive solar still (Fig. 23(a)). The hybrid active solar still gives around 3.5 times higher annual yield (1203.46 kg) than the passive solar still (343.36 kg). The

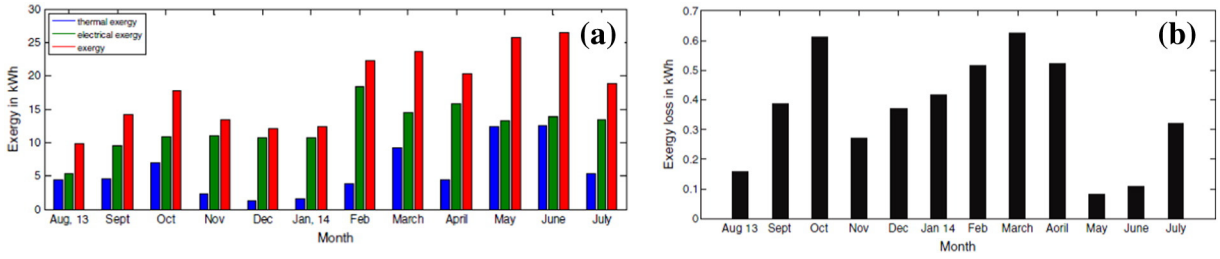

Fig. 22. Monthly variation of (a) exergy and (b) exergy loss of the system (follow Tiwari et al. [67] for Table 2(a–c)).

variation of *CPK* of distilled water with respect to their designed life (n), at different maintenance cost, capital cost, and for fixed interest rate ($i = 4\%$) for passive and hybrid (PV/T) active solar still are shown in Fig. 23(b) and (c) respectively. It has been found that CPK increases by 10% on raising the maintenance cost up 15%. In general, at 4% interest rate, the production cost of distillate reduces to 33% if life of the passive solar still raises by 100%, irrespective of the maintenance cost. From figure, it has been observed that the minimum costs estimated for the proposed passive and hybrid active solar stills are respectively *Rs*.0.70/kg and *Rs*.1.94/kg.

The payback period reduces significantly on increasing the selling price from *Rs*.2.0/kg to *Rs*.6.0/kg (Fig. 23(d)). It is found to be 6.2 years and 23.9 years for the passive and hybrid (PV/T) solar still respectively for *Rs*.2.0/kg marketing selling rate and 4% interest rate. The clear number of days in a year, high solar radiation, and larger sunshine hours period significantly reduces the production cost and pay back periods. The EPBT of the proposed passive and hybrid (PV/T) active solar stills are found to be 2.9 years and 4.7 years, respectively.

3.9. Evacuated tubular collector (ETC) coupled solar still in natural mode [77]

Systematic diagram of water-in-glass evacuated tubular solar collector is presented in Fig. 24(a). The system comprises of single slope solar still (area 1 $m^2$and glass cover angle 30°) and water-in-tube evacuated tubular collector (ETC). The solar still of is made of fibre reinforced plastic (FRP) and mounted on iron stand. The basin surface from the inner side is painted mat black to enhance the absorptivity of the surface to absorb the maximum solar radiation as explained earlier. An evacuated tubular collector (ETC) comprises of a number of concentric borosilicate tubes (*length* 1.4 m; *diameter* 0.044 m) are mounted over a diffuse reflector with center-line spacing of 0.07*m* inclined at an angle of 45° from horizontal. The inner surface of the tubes is blackened and the selective coating is used on the outer surface to enhance the absorptivity. The tubes transfer the heat to the water flowing inside it through the contact peripheral surface. The hot water rises up due to low density whereas the cold water takes its place due to gravity and high density

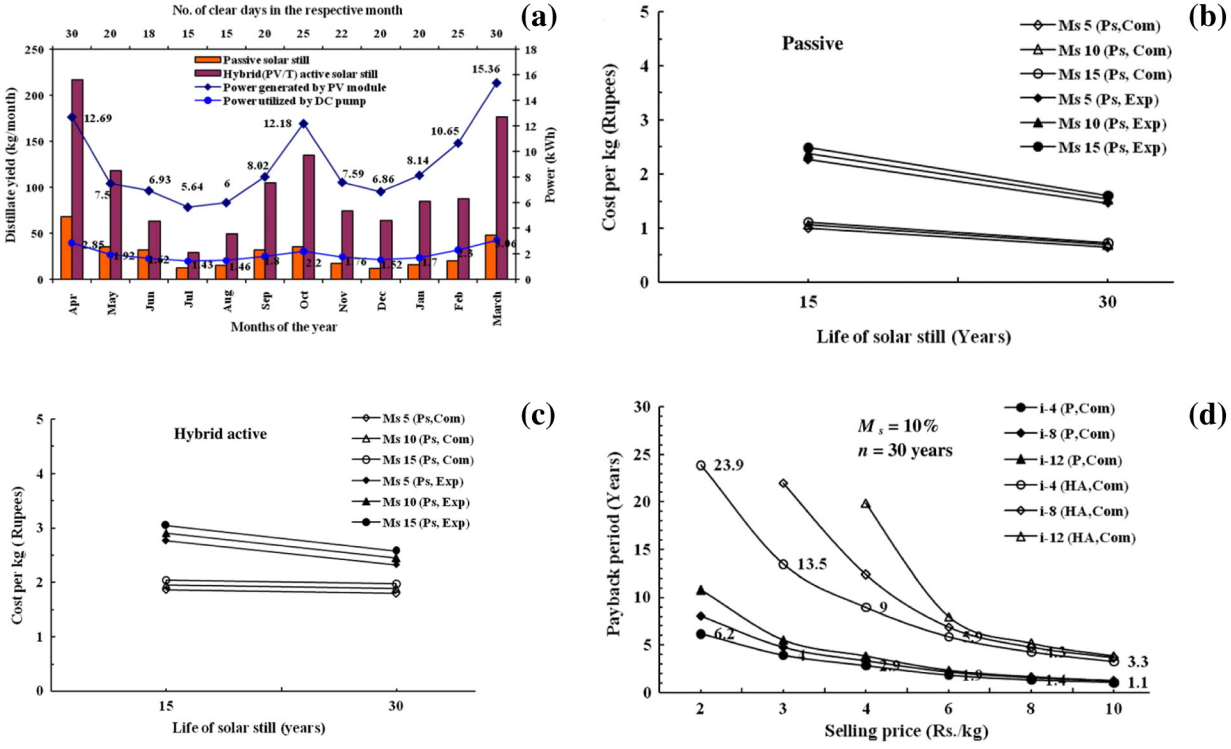

Fig. 23. (a) Monthly yield obtained from passive and hybrid (PV/T) active solar still for 0.05 *m* water depths and power generated by PV module. Variation of cost per kg (CPK) of distilled water with respect to their designed life (n), at different maintenance cost, capital cost, and for fixed interest rate ($i = 4\%$) for (b) passive and (c) hybrid (PV/T) active solar still. (d) Variation of payback periods with selling price for proposed passive and hybrid (PV/T) active solar stills for designed life span of 30 years.

Please cite this article as: G.N. Tiwari, L. Sahota, Review on the energy and economic efficiencies of passive and active solar distillation systems, Desalination (2016), http://dx.doi.org/10.1016/j.desal.2016.08.023

from solar still as shown in Fig. 24(b). The instantaneous solar energy input, fluid temperature, and collector configuration affects the circulation flow rate inside the collector loop. The orientation of the water-in-tube evacuated tubular collector coupled with single slope solar still (ETC-SSSS) system is placed in due south to retrieve the maximum solar radiation throughout the year. The external thermal energy (hot water) from the outlet of the evacuated tubular collector is fed into the basin of the still. Hence, it improves the rate of evaporative heat transfer from the surface of basin water. The yield of the hybrid active system can be further improved by lowering the temperature of the condensing cover.

Singh et al. [77] theoretically presented the thermal analysis of the system discussed and they optimized it for the integrated evacuated tubes, basin water temperature, and the basin water depth. The performance (yield; energy and exergy efficiencies; glass cover and basin water temperatures) has been analyzed for a typical summer day of New Delhi climatic conditions.

Following Singh et al. [77], the energy balances for different components of ETC-SSSS system can be written as

(i) Glass cover

$$\alpha_g I_S(t)A_g + h_{1w}(T_{sw}-T_{gi})A_b = h_{1g}(T_{go}-T_a)A_g \tag{81}$$

(ii) Bain liner

$$\alpha_b I_S(t)A_b = h_{bw}(T_{sw}-T_{gi})A_b + h_{ba}(T_b-T_a)A_b \tag{82}$$

(iii) Water mass in solar still

The rate of thermal energy available at the outlet of water-in-tube ETC is fed into solar conventional still. The energy balance of the water mass inside the still can be expressed as;

$$N_c(\dot{m}C_w)(T_{cw}-T_{sw}) + \alpha_w A_b I_s(t) + h_{bw}(T_b-T_{sw})A_b = h_{1w}(T_{sw}-T_{gi})A_b + (M_{sw}C_w)\frac{dT_{sw}}{dt} \tag{83}$$

(iv) Water mass in evacuated tubes

$$N_c A_t I_s(t)\eta_0 + \alpha_w N_c A_t (T_{cw}-T_a) = N_c(\dot{m}C_w)(T_{cw}-T_{sw}) + (M_{cw}C_w)\frac{dT_{cw}}{dt} \tag{84}$$

Solving above equations, one can get

$$\frac{dT_{cw}}{dt} + a_1 T_{cw} + b_1 T_{sw} = g_1(t) \tag{85}$$

$$\frac{dT_{sw}}{dt} + a_2 T_{cw} + b_2 T_{sw} = g_2(t) \tag{86}$$

The values of T_{cw} and T_{sw} can be obtained by solving Eq. (85) and Eq. (86) respectively.

All the unknowns in above equations are given in Appendix A [77].

The circumferential heat flow rate in the tube water can be expressed as

$$\dot{m} = \frac{\pi d_t \mu (Re)}{4} = 0.048(\pi d_t \mu)\left[\frac{Nu.Gr}{Pr}\cos(\theta)\left(\frac{1}{d_t}\right)^{1.2}\right]^{0.4084} \tag{87}$$

The instantaneous exergy efficiency of the system can be expressed as

$$\eta_{is} = \frac{h_{sw}(T_{sw}-T_{gi})A_b}{I_s(t)A_b + I_c(t)A_a} \tag{88}$$

The exergy output of the solar still can be expressed as

$$\dot{E}_{X,evap} = h_{ew} A_b (T_{sw}-T_{gi})\left(1-\frac{T_a}{T_{sw}}\right) \tag{89}$$

The energy efficiency has been found higher for the lower water depths and it found to be maximum (119.4%) around 16:00 h. Energy efficiency of the solar still slows its enhancement rate during the early hours of the day due to an increase in the heat flow to brackish water as compared to the heat of evaporation. The maximum value of instantaneous exergy efficiency has been found to be 18.2% for 0.03 m water depth. A part of incoming solar exergy is being destroyed due to irreversibility in different components. The increase in irreversibility lowers the exergy efficiency. It has been found that the evaporative exergy fraction dominates over the convective and radiative exergy fractions (Fig. 25(a)) and it is found to be >50% most of the times in 24hs. For a combination of 10 ETCs and 0.03 m basin water depth, the maximum daily energy (33.0%) and exergy (2.5%) efficiencies are found (Fig. 25(b)). Daily energy and exergy efficiencies decrease significantly on increasing the water depth as shown in figure. The combination among the ETC size and basin water depth needs adjustment to make the system efficient. Smaller size of ETC with 10 number of tubes is preferable than a single unit of the larger size of integrated ETC.

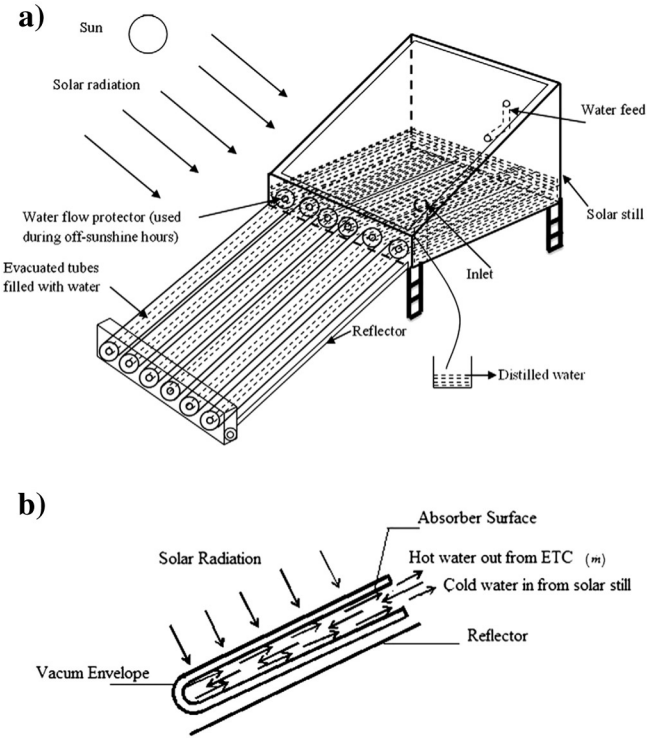

Fig. 24. (a) Schematic diagram of evacuated tubular collector integrated with single slope solar still (ETC-SSSS) in natural mode, (b) Schematic diagram of thermo syphon process in single tube.

3.10. Evacuated tubular collector (ETC) coupled solar still in forced mode [78]

The system description is similar to that of ETC-SSSS system operated in natural mode (Section 3.9) except the incorporated DC water pump to circulate water in the present system. A check valve is provided in the pipe line to avoid the reverse flow during nighttime.

Kumar et al. [78] presented the thermal modeling of tube-in-water evacuated tubular collector integrated with single slope solar still (ETC-SSSS) in forced mode operation (Fig. 26). The analysis has been carried out for climatic conditions of the New Delhi. They optimized the coupled system for the mass flow rate and basin water depth. The daily yield, energy and exergy efficiency, and the economic analysis of the system have been investigated by Kumar et al. [78].

Kumar et al. [78], energy balances of different components of the coupled system are given as

(i) Glass cover

$$\alpha_g I_S(t)A_g + h_{1w}(T_{sw}-T_{gi})A_b = h_{1g}(T_{go}-T_a)A_g \tag{90}$$

(ii) Bain liner

$$\alpha_b I_S(t)A_b = h_{bw}(T_{sw}-T_{gi})A_b + h_{ba}(T_b-T_a)A_b \tag{91}$$

(iii) Water mass in solar still

$$(\dot{m}C_w)(T_{cw}-T_{sw}) + \alpha_w A_b I_s(t) + h_{bw}(T_b-T_{sw})A_b = h_{1w}(T_{sw}-T_{gi})A_b + (M_{sw}C_w)\frac{dT_{sw}}{dt} \tag{92}$$

(iv) Water mass in evacuated tubes

$$h_{tw}A_t(T_t-T_{cw})N_c = (\dot{m}C_w)(T_{cw}-T_{sw}) + (M_{cw}C_w)\frac{dT_{cw}}{dt} \tag{93}$$

(v) Water-in-glass evacuated tubes

$$\alpha_t\left(\frac{A_t}{2}\right)I_c(t)N_c(1+\rho_r) = h_{tw}(T_t-T_{cw}) + h_{ta}A_t(T_t-T_a)N_c \tag{94}$$

Solving above equations, one can get

$$\frac{dT_{cw}}{dt} + a_1T_{cw} + b_1T_{sw} = g_1(t) \tag{95}$$

$$\frac{dT_{sw}}{dt} + a_2T_{cw} + b_2T_{sw} = g_2(t) \tag{96}$$

All the unknowns in above equations are given in Appendix A [78].

The instantaneous exergy efficiency of the ETC-SSSS system (η_{is}) operated in forced mode condition can be expressed as

$$\eta_{is} = \frac{h_{sw}(T_{sw}-T_{gi})A_b}{I_s(t)A_b + I_c(t)A_a} = \frac{M_eL}{[I_s(t)A_b + I_c(t)A_a]\times 3600} \tag{97}$$

The exergy output of the solar still can be expressed as

$$\dot{E}_{X,evap} = h_{ew}A_b(T_{sw}-T_{gi})\left(1-\frac{T_a}{T_{sw}}\right) \tag{98}$$

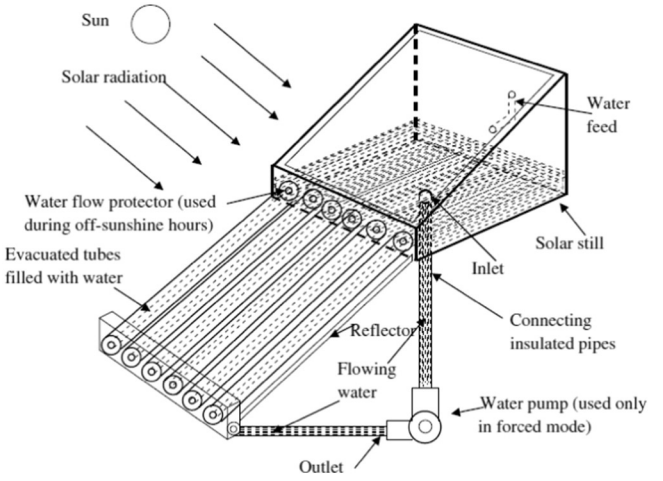

Fig. 26. Schematic view of tube-in-water evacuated tubular collector integrated with single slope solar still (ETC-SSSS) in forced mode condition.

The maximum water temperature (83.0 – 92.6 °C) and daily yield (2.57 – 3.47 kg) obtained from the system varies significantly on changing mass flow rate from 0.001 kg/s to 0.006 kg/s. It has been observed that both energy and exergy efficiencies increases with increase in mass flow rate and found to be maximum (energy 30.02%; exergy 1.75%) at 0.006 kg/s mass flow rate (Fig. 27(a)). On the other hand, the hourly variation (during sunshine hours) of instantaneous energy and exergy output is found to be higher at lower water depth (0.03 m). Eventually, the optimum mass flow rate of 0.06 kg/s has been evaluated at 0.03 m basin water depth and this combination produces daily yield of 3.9 kg/m^2 which is significantly higher than the yield predicted for the same configuration of the system operating in natural mode.

The annual average yield (567.3 kg/m^2) of ETC-SSSS in forced mode condition has been found to be marginally higher than the ETC-SSSS operated in natural mode (Fig. 27(b)). The annual average yield (263.6 kg/m^2) obtained from the hybrid (PV-T) active solar still is significantly lower than the yield obtained from the ETC-SSSS system due to higher losses of convection in FPCs. On the other hand, the average annual values of evaporative HTC of ETC-SSSS (forced mode) are also found to be approximately 1.5 times higher in comparison to the hybrid (PV/T) active solar still. The cost payback period is also found to be lower than the hybrid (PV-T) active solar still for Rs. 6.0/kg selling price of the distillated water in the market.

4. Solar stills: a review of the latest developments in numerical simulations [79]

Edalatpour et al. [79] reported a review on the latest developments in latest simulations of solar stills. Complexity, time consumption, and

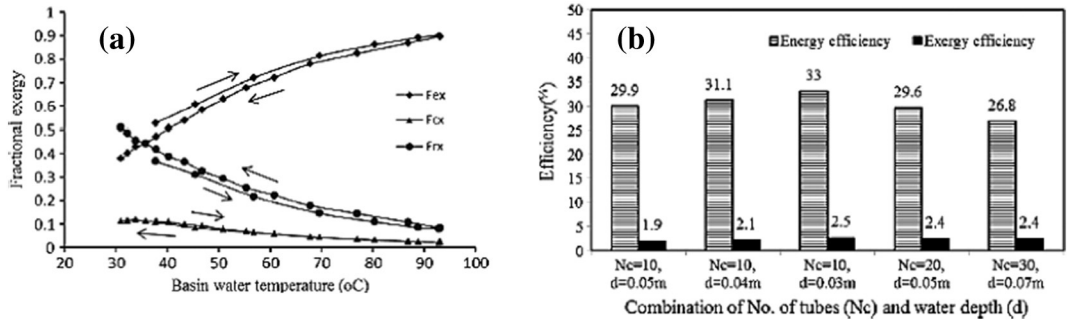

Fig. 25. (a) Variation of fraction exergy with basin water temperature, and (b) energy and exergy efficiency of with different set of combinations.

cost processes to establish the solar desalination systems forced researchers to study these systems analytically (mathematical and numerical simulations) using computer software viz. FLUENT, MATLAB, FORTRAN etc. In the review, the multiplicity of new developments in water purification processes through mathematical and numerical modeling has been presented. Such developments or improvements comprises of designing novel, adding additional tools to amplify water yield as well as altering operating and influential parameters to attain more fresh water. Summary of recent numerical studies on solar stills are given in the comprehensive review presented by Edalatpour et al. [79].

Edalatpour et al. provided the following new, complete and comprehensive details of the significant desalination systems;

(i) Mathematical model deployed for a single slope solar still coupled a compression heat pump.

(ii) Latest developments for the different solar stills:

Single slope solar still

(a) Hybrid (PV/T) active solar still [61]

(b) Active single slope solar still coupled with shallow solar pond [80]

(c) Solar still coupled with evacuated tubular collector [77]

(d) Modified single slope solar still [81]

(e) Capillary film solar still [82]

Double slope solar still

(a) Active double slope solar still [63]

(b) Double slope double basin solar still [83]

(c) Asymmetric solar still [84]

Stepped solar still [85,86], Tubular solar still [87], Modified solar still [88–90], Cascade solar still [91,92], and other designs [93–100].

Following conclusions has been withdrawn after reviewing different types of solar stills:

Single slope solar still: (i) The system yield can be enhanced significantly on coupling the conventional solar still with shallow solar pond, external reflectors, PV/T tank, evacuated tubular collectors, and compression heat pump. (ii) Inclination of external reflector should backward in summer season and forward in other seasons. (iii) Water depth and water mass flow rate have a converse effect on system yield. The insulation thickness marginally affects the yield. (iv) Blade installation inside the still mitigates the yield.

Double slope solar still: (i) Water depth and material used for the still construction have nasty effect on the system yield. (ii) It is more economical and sustainable as well as it has higher exergy efficiency in comparison to the single slope solar still.

Multi-effect solar still: (i) The system yield can be enhanced by including the corrugated shape stacked trays, heat pump, and thermal energy storage tank. (ii) The heat losses and condensation resistance can be minimized by using vertical ripples.

Cascade solar still: (i) Phase changing material inclusion enhance the system production rate. (ii) Increase in aspect ratio and water depth reduces the system yield.

Stepped solar still: (i) Depth and width of the tray significantly affects the system yield. (ii) The system yield increases on operating internal reflectors.

5. Solar stills with nanofluids: a recent approach

Nanofluids, a combination of metallic nanoparticles and basefluid, are the new generation of ultrafast heat transfer fluids due to their exceptional thermo-physical (thermal conductivity, specific heat, density, dynamic viscosity etc.) and optical properties. Nanofluids are proficient for harvesting thermal energy in solar thermal applications. Worldwide, nanofluids attract an attention of researchers and engineers to utilize their ultrafast heat transfer abilities for various applications in engineering science and technology. The most important step is to elect a suitable heat transfer nanofluid for the desired application. The working principle of passive double slope solar (DSSS) still incorporating nanofluids has been described below;

The schematic diagram of passive DSSS with nanofluid is shown in Fig. 28. Suspension of metallic nanoparticles in the basefluid of passive DSSS improves its heat transfer rate and optical properties. The improvement in heat transfer ability is credited to the enhanced thermophysical properties of nanoparticles. The transmitted solar radiation through transparent condensing cover inside the solar still gets first attenuated (absorbed) by the nanofluid and then finally absorbed by blackened surface (basin liner). The plasmon resonance absorption band of metallic nanoparticles arises in the visible and near IR spectrum. Therefore, the mixed metallic nanoparticles in the basefluid directly absorb the solar radiation due to matching between its optical absorption spectrum and the solar radiation spectrum. By absorbing solar radiation directly, each individual metallic nanoparticle's temperature enhances and hence thermal conductivity (dominating property of nanofluids among others) which intern enhances the fluid temperature. Consequently, the mutual effect of transfer of energy from metallic nanoparticles and basin liner raises the temperature of the nanofluid in passive DSSS. It leads to the raise the temperature gap among the evaporative (nanofluid) surface and inner surface of the transparent condensing cover which acts as a driving force for distillation. Eventually, through the mechanism of heat transfer, evaporated water reaches on the inner surface of the condensing cover and gets condensed there after releasing its latent heat to the condensing cover. The condensed water trickles into the channels provided at the lower ends of the glass cover under gravity [101].

5.1. Passive double slope solar still (DSSS) with Al_2O_3 nanoparticles [102]

Sahota and Tiwari [102] studied the performance of passive double slope solar still (DSSS) by incorporating Al_2O_3 metallic nanoparticles for two different water depths (35 kg and 80 kg) for the climatic conditions of New Delhi for the month March 2015. The analysis has been carried out for the basefluid (water only) as well as for the nanofluid with

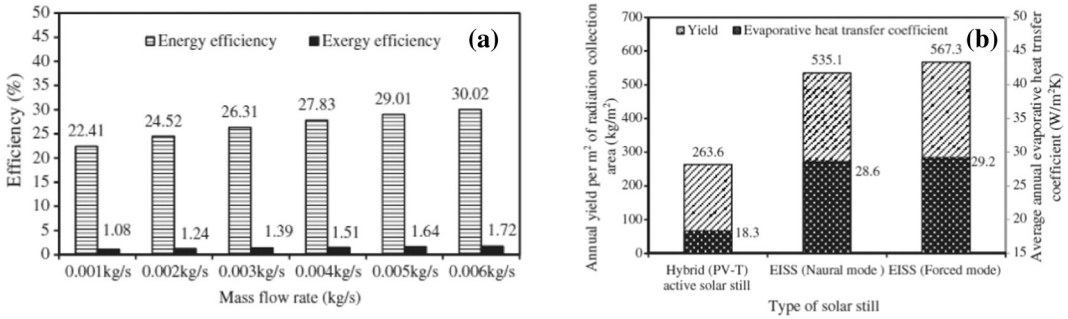

Fig. 27. (a) Variation of energy and exergy efficiency with mass flow rate, (b) annual yield and annual average heat transfer coefficient for different systems.

Please cite this article as: G.N. Tiwari, L. Sahota, Review on the energy and economic efficiencies of passive and active solar distillation systems, Desalination (2016), http://dx.doi.org/10.1016/j.desal.2016.08.023

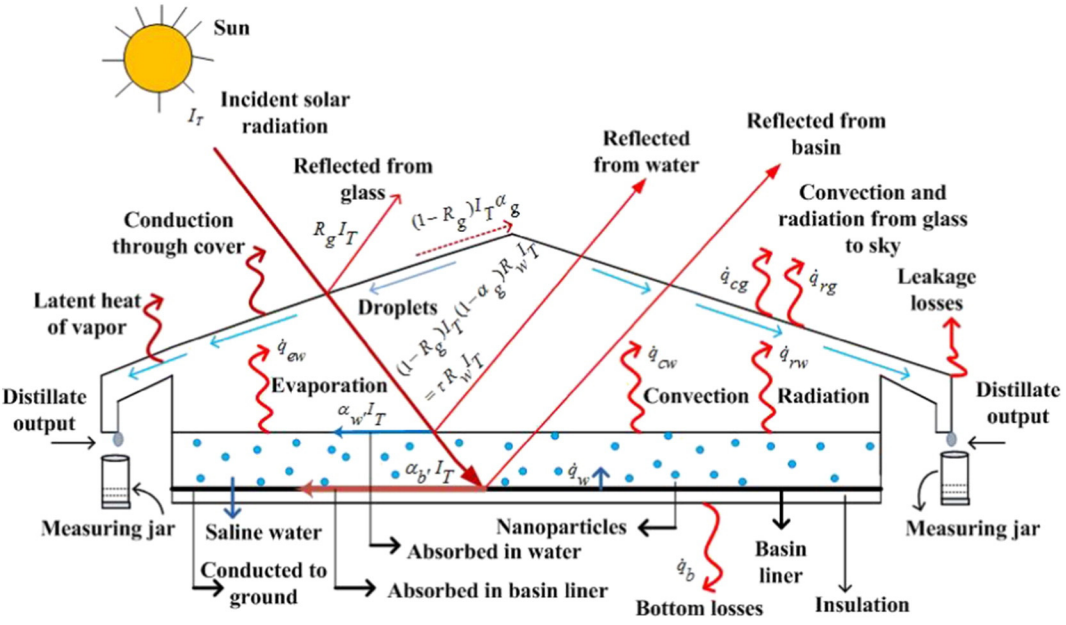

Fig. 28. Passive double slope solar still with nanofluid.

three different concentrations (0.04%, 0.08% and 0.12%). Effect of different concentrations of Al_2O_3 nanoparticle on fluid temperature, thermal conductivity, internal heat transfer coefficients (HTC), and yield of the fluid (BF/NF) has been studied by Sahota and Tiwari.

Following Sahota and Tiwari [102];

$$T_{bf} = \frac{\overline{f'(t)}}{a}\left[1-e^{-a\Delta t}\right] + T_{bf0}\, e^{-a\Delta t} \tag{99}$$

The unknowns in above equation are given in Appendix A [102].

The peak value of the maximum temperature difference originates around 35 kg basefluid mass available in the still and it increases with increase in concentration of Al_2O_3 metallic nanoparticles (Fig. 29(a)). The same variation has also been observed on reducing the solar intensity by 30% but the maxima for all three different concentrations of metallic nanoparticles has been shifted towards the lower end (around 20 kg) of the basefluid mass (kg) available in the still (Fig. 29(b)). The daily yield obtained from nanofluid increases on increasing the metallic nanoparticle concentration for both east and west side of the system. The yield obtained from the east condensing glass cover was marginally higher compared to the west condensing glass cover. Significant enhancement in the daily yield from 35 kg (12.2%) and 80 kg (8.4%) basefluid mass has been found at 0.12% concentration of Al_2O_3 metallic nanoparticles in comparison to the basefluid (water).

5.2. Passive double slope solar still (DSSS) with different nanofluids: a comparative study using characteristic curve [103]

Working of the passive double slope solar still with nanofluids has been explained earlier in Section 5. Sahota and Tiwari [103] presented an analytical expression of the characteristic equation of passive double slope solar still (DSSS) for Al_2O_3, TiO_2, and CuO-water based nanofluids for New Delhi climatic conditions for the month March 2015. The analysis has been carried out for the optimized concentration (0.25%) of metallic nanoparticles and fluid (NF/NF) mass. Furthermore, they estimated the system yield for different weather conditions of the month March using the proposed model.

Following Sahota and Tiwari [103], hourly thermal energy and exergy of the system are given as

$$E_{hourly,en} = \left[h_{ebf,E}\left(T_{bf}-T_{giE}\right) + h_{ebf,W}\left(T_{bf}-T_{giW}\right)\right]A_b \tag{100}$$

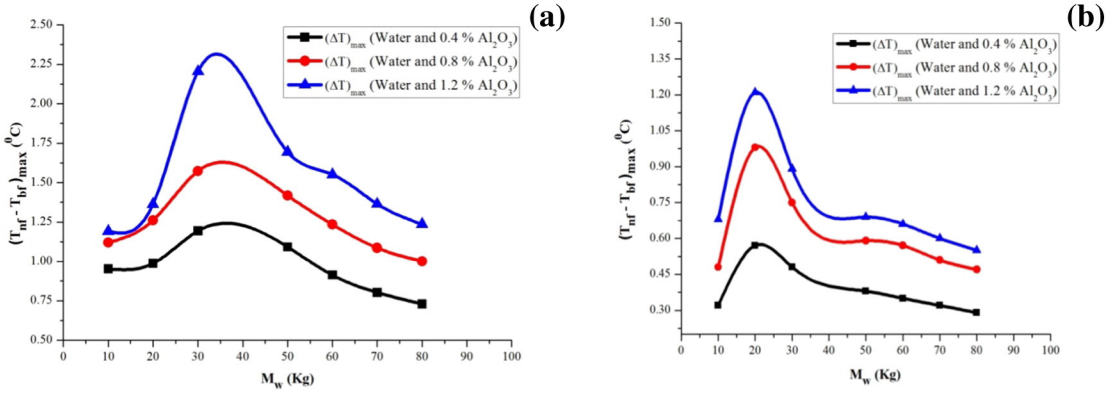

Fig. 29. Variation maximum temperature difference among the basefluid (water) and nanofluid with fluid mass for different concentrations (0.04%, 0.08%, *and* 0.12%) of Al_2O_3 nanoparticles of passive DSSS for (a) solar intensity of month March 2015 and (b) 30% lower solar intensity.

$$E_{hourly,ex} = \left\{ h_{ebf,E}\left[(T_{bf} - T_{giE}) - (T_a + 273)\ln\left(\frac{T_{bf}+273}{T_{giE}+273}\right)\right] + h_{ebf,W}\left[(T_{bf} - T_{giW}) - (T_a + 273)\ln\left(\frac{T_{bf}+273}{T_{giW}+273}\right)\right]\right\} A_b \quad (101)$$

Instantaneous gain thermal energy efficiency (η_{th}) can be written as

$$\eta_{th} = F'\left[(\alpha\tau)_{eff} + \frac{(T_{bf0} - T_a)}{I(t)} U_{eff}\right] \quad (102)$$

The lost thermal energy efficiency of passive DSSS is obtained as

$$\eta_{L,th} = F'_L\left[(\alpha\tau)_{eff} - U'_{eff}\frac{(T_{bfo} - T_a)}{I(t)}\right] \quad (103)$$

where, the unknowns in Eq. (102) and Eq. (103) are given in appendix A [103].

For given parameters of the system, the variation η_{th} and $\eta_{L,th}$ with reduced temperature $((T_{bf0} - T_a)/I(t))$ gives the instantaneous thermal gain energy efficiency and thermal loss energy efficiency respectively. The analysis of energy and exergy are carried out on the basis of first and second law of thermodynamics respectively.

The hourly thermal exergy efficiency of passive DSSS is obtained from the following modified equation;

$$\eta_{hourly,ex} = \left(\frac{1}{0.933 \times A_s \times I_s(t)}\right)\left\{ h_{ebf,E}\left[(T_{bf} - T_{giE}) - (T_a + 273)\ln\left(\frac{T_{bf}+273}{T_{giE}+273}\right)\right] + h_{ebf,W}\left[(T_{bf} - T_{giW}) - (T_a + 273)\ln\left(\frac{T_{bf}+273}{T_{giW}+273}\right)\right]\right\} A_b \quad (104)$$

It has been observed value of maximum temperature difference increases with an increase in the concentration of all three different nanoparticles only up to 0.25% (concentration) and then it starts decreasing. The optimized concentration 0.25% of Al_2O_3, TiO_2, and CuO nanoparticles has been found at 35 kg fluid (BF/NF) mass. The maximum values of instantaneous thermal energy efficiency (η_{th}) for all three water based nanofluids has been found significantly higher than the thermal energy efficiency of the system obtained with basefluid only (Fig. 30(a)). It is due to the enhanced thermo-physical properties of nanofluid. Again the thermal losses are also higher for the nanofluids compared to basefluid (Fig. 30(b)). The maximum value of (a) instantaneous thermal energy efficiency (η_{th}) observed is 50.34%, 46.10%, and 43.81% and (b) thermal exergy efficiency is 14.10%, 12.38%, and 9.75% for Al_2O_3, TiO_2, and CuO-water based nanofluid respectively for passive DSSS system. The thermal exergy has also been found higher for nanofluids (Al_2O_3 14.10%; TiO_2 12.38%; and CuO 9.75%) as compared to basefluid (4.92%). The yield of passive DSSS is obtained higher for Al_2O_3-water based nanofluid from the east and west side. It is also found to be higher for c-type of weather conditions (marginally higher than the d-type) for both east and west side of the system.

5.3. Internal heat transfer coefficients (HTCs) in passive double slope solar still (DSSS) with different nanofluids [104]

Sahota and Tiwari [104] studied the internal heat transfer coefficients (evaporative, convective, and radiative), Nusselt number, and energy fractions of passive DSSS for the optimized concentration (0.25%) of metallic nanoparticles (Al_2O_3, TiO_2 and CuO) and fluid (BF/NF) mass (35 kg). Different heat transfer coefficients (Table 4) can be evaluated using the thermo-physical properties of the basefluid (Table 2) and water based nanofluid (Table 3).

Radiative HTC of east and west side of condensing cover is given as

$$h_{rgE} = \frac{\epsilon_g\sigma\left[(T_{giE}+273)^4 - (T_{sky}+273)^4\right]}{(T_g - T_a)}; h_{rgW} = \frac{\epsilon_g\sigma\left[(T_{giW}+273)^4 - (T_{sky}+273)^4\right]}{(T_g - T_a)} \quad (105)$$

where, $T_{sky} = T_a - 6$

From Cooper and Dunkle model, the generalized expression of internal evaporative and convective heat transfer coefficients are given below as

$$h_{ef} = (0.016273)h_{cf}\left[\frac{P_f - P_{gi}}{T_f - T_{gi}}\right]; \text{and } h_{cf} = (0.844)(\Delta T)^{1/3} \quad (106)$$

where; $P_x = exp[25.317 - (\frac{5144}{T_x+273})]$; $\Delta T = (T_f - T_{gi}) + [\frac{(P_f - P_{gi})(T_f+273)}{2.689\times10^5 - P_f}]$.

The fluid temperature (T_f) is given in Eq. (99).

Internal radiative heat transfer coefficient is given as

$$h_{rf} = \epsilon_{eff}\sigma\left[(T_f+273)^4 + (T_{gi}+273)^4\right][T_f + T_{gi} + 546] \quad (107)$$

The natural convective heat transfer coefficient (h_{nc}) from basin to fluid surface has been obtained from the following relation of Nusselt

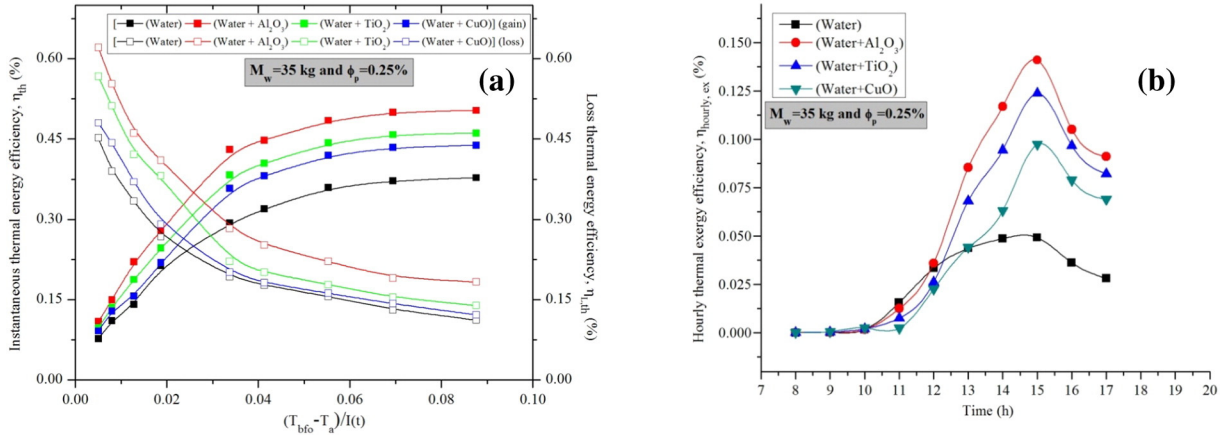

Fig. 30. (a) Variation of instantaneous thermal efficiency (η_{th}) and loss thermal energy efficiency ($\eta_{L,th}$) with reduced temperature $((T_{bf0} - T_a)/I(t))$, and (b) hourly variation of instantaneous thermal exergy efficiency for basefluid (water) and nanofluid (Al_2O_3,TiO_2, and CuO nanoparticles) for 0.25% concentration of nanoparticles and 35 kg fluid (BF/NF) mass.

Please cite this article as: G.N. Tiwari, L. Sahota, Review on the energy and economic efficiencies of passive and active solar distillation systems, Desalination (2016), http://dx.doi.org/10.1016/j.desal.2016.08.023

Table 2
Thermo-physical properties of basefluid [108].

Quantity	Symbol	Expression
Density	ρ_{bf}	$999.79+0.0683\times T_{bf}-0.0107\times T_{bf}^2+0.00082\times T_{bf}^{2.5}-2.303\times10^{-5}\times T_{bf}^3$
Specific heat	C_{bf}	$4.217-0.00561\times T_{bf}+0.00129\times T_{bf}^{1.5}-0.000115\times T_{bf}^2+4.149\times10^{-6}\times T_{bf}^{2.5}$
Viscosity	μ_{bf}	$\frac{1}{(557.82-19.408\times T_{bf}+0.136\times T_{bf}^2-3.116\times10^{-4}\times T_{bf}^3)}$
Thermal conductivity	k_{bf}	$0.565+0.00263\times T_{bf}-0.000125\times T_{bf}^{1.5}-1.515\times10^{-6}\times T_{bf}^2-0.000941\times T_{bf}^{0.5}$

Table 3
Thermo-physical properties of Al_2O_3-water based nanofluid.

Model/correlation	Quantity	Expression
Pak and Cho [109]	Specific heat	$C_{nf}=\frac{[(\varphi_p\ \rho_p C_p+(1-\varphi_p)\ \rho_{bf}C_{bf})]}{\rho_{bf}}$; $\varphi_p=\frac{V_p}{V_f+V_p}$; Here, 'V' is the volume.
Pak and Cho [109]	Density	$\rho_{nf}=\varphi_p\rho_p+(1-\varphi_p)\rho_{bf}$
Khanafer and Vafai [110]	Thermal conductivity	$k_{nf}=k_{bf}[1+(1.0112)\varphi_p+(2.4375)\varphi_p(\frac{47}{d_p(nm)})-(0.0248)\varphi_p(\frac{k_p}{0.613})]$
Khanafer and Vafai [110]	Viscosity	$\mu_{nf}=-0.4491+(\frac{28.837}{T_{nf}})+0.547\varphi_p-0.163\varphi_p^2+(23.653)(\frac{\varphi_p}{T_{nf}})^2+(0.0132)\ \varphi_p^3-(2354.7)(\frac{\varphi_p}{T_{nf}^2})+(23.498)(\frac{\varphi_p}{d})^2-(3.018)(\frac{\varphi_p^3}{d_p^2})$ $11\le\varphi_p\le9;13\le d_p\le130nm;20\le T\le70\ ^\circ C$
Wang et al. [111] and Ho et al. [112]	Thermal expansion coefficient	$\beta_{nf}=(1-\varphi_p)\beta_{bf}+\varphi_p\beta_p$

number (Nu);

$$(Nu)_f=\frac{h_{nc}X}{K}=C(GrPr)^n \tag{108}$$

For horizontal plate facing upward, $C=0.54$ and $n=¼$.

The generalized expression of convection, radiation, and evaporation energy fractions of fluid (BF/NF) are given as

$$F_{cf}=\frac{\dot{Q}_{cf}}{\dot{Q}_1};\ F_{rf}=\frac{\dot{Q}_{rf}}{\dot{Q}_1};\ F_{ef}=\frac{\dot{Q}_{ef}}{\dot{Q}_1} \tag{109}$$

The hourly variation of natural convective heat transfer coefficient of passive DSSS system for basefluid and Al_2O_3, TiO_2 and CuO-water based nanofluids have been presented in Fig. 31(a). It improves around 2–3 times for all three nanofluids in comparison to the basefluid. The Nusselt number (Nu) has been also found to be 2–3 times higher for Al_2O_3, TiO_2 and CuO-water based nanofluids in comparison to the basefluid (water) (Fig. 31(b)). The variation of Nusselt number with fluid (BF/NF) temperature for the basefluid and all three different nanofluids is also presented in Fig. 32. It has been perceived that the Nusselt number increases with increase in fluid (BF/NF) temperature and found to be higher for all three nanofluids in comparison to the basefluid. It is credited to the fact that Nusselt number directly depends on the natural convective heat transfer coefficient which further depends on the basin geometry (Constants C and n), absorptivity of the basin, and thermal conductivity. Therefore, higher values of Nusselt number implies the higher convective heat transfer coefficient form the basin/blackened surface to the basin fluid (BF/NF).

The Nusselt number obtained for basefluid of the DSSS system increases rapidly in the range of 60 °C − 70 °C. At higher temperature range, it has been found that the Nusselt number for basefluied of the system starts approaching the values of the Nusselt number obtained for the water based all three different nanofluids. The hourly variation of internal evaporative, convective, and radiative heat transfer coefficients (HTCs) obtained with basefluid and Al_2O_3, TiO_2 and CuO-water based nanofluids from the east and west side of the passive DSSS system is presented in Fig. 33. The peak or maxima of all the curves of HTCs obtained with basefluid and nanofluids originates during sunshine hours. It has been observed that the HTCs obtained from the west side of the

Table 4
Generalized formulas of different heat transfer coefficients used in thermal modeling of passive DSSS.

	Relations	Heat transfer coefficient
Nusselt number	$(Nu)_f=\frac{hX}{k}=C(GrPr)^n$ Grashof number $(Gr)_f=[\frac{g\beta\rho^2L^3\Delta T}{\mu^2}]_f$ Prandtl number $(\ ,Pr)_f=(\frac{\mu C_p}{k})_f$ Rayleigh number $(Ra)_f=(GrPr)_f=[\frac{g\beta\rho^2C_pL^3\Delta T}{\mu k}]_f$ C = 0.54 and n = ¼ horizontal plate facing upward	It provides the convective HTC from the horizontal basefluid surface in the upward direction
Cooper and Dunkle model [50]	$h_{ef}=(0.016273)h_{cf}[\frac{P_f-P_{gi}}{T_f-T_{gi}}]$ $h_{cf}=(0.844)(\Delta T)^{1/3}$ Here; $P(x)=\ ,exp[25.317-(\frac{5144}{T(x)+273})]$ $\Delta T=(T_f-T_{gi})+[\frac{(P_f-P_{gi})(T_f+273)}{2.689\times10^5-P_f}]$	Internal evaporative and HTC from fluid to glass surface
Radiative HTC	$h_{rf}=\in_{eff}\sigma[(T_f+273)^4+(T_{gi}+273)^4][T_f+T_{gi}+546]$ Here; $\frac{1}{\in_{eff}}=\frac{1}{\in_w}+\frac{1}{\in_g}-1$	Internal radiative HTC from fluid to glass surface
Total external HTC	$h_0=5.7+3.8V$ $h_i=2.8+3V$ Where V is wind velocity	External HTC from condensing surface to ambient

Please cite this article as: G.N. Tiwari, L. Sahota, Review on the energy and economic efficiencies of passive and active solar distillation systems, Desalination (2016), http://dx.doi.org/10.1016/j.desal.2016.08.023

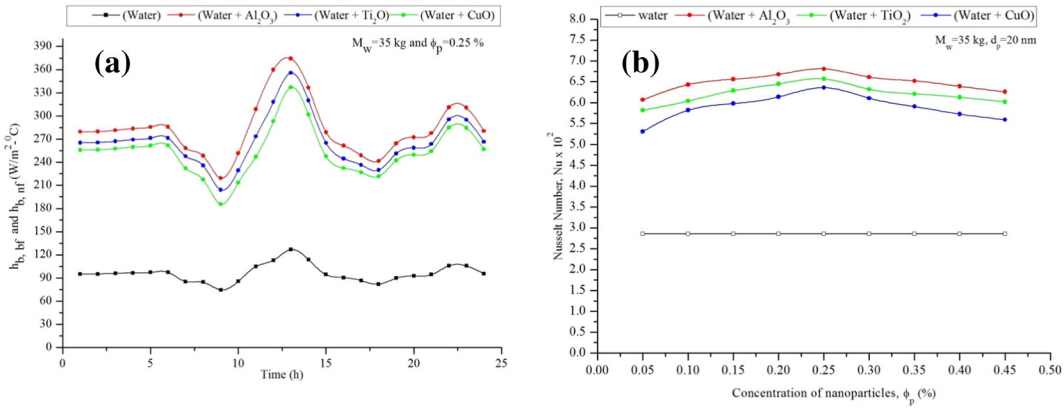

Fig. 31. (a) Hourly variation of natural convective heat transfer coefficient (basin liner to fluid) for basefluid (water) and Al_2O_3, TiO_2, and CuO-water based nanofluids at 0.25% concentration, and (b) variation of Nusselt number with concentration of metallic nanoparticles (Al_2O_3, TiO_2, and CuO).

still are marginally higher than the east side. The significant enhancement in the evaporative HTC is observed for both east and west side of the system for all three nanofluids in comparison to the basefluid. This is due to the enhanced surface area for heat transfer from metallic nanoparticles to assisting fluid at higher concentration of the assisting metallic nanoparticles. Consequently, the temperature of the nanofluid increases and hence the internal HTCs as explained earlier. Significant enhancement of 46.97%, 31.22%, and 12.9% from the east side and 51.80%, 37.35%, and 20.6% from the west side has been observed in the evaporative HTC with the Al_2O_3, TiO_2 and CuO-water based nanofluids respectively. On the other hand, the radiative and convective energy fraction dominates at lower temperature while the evaporative energy fraction dominates at higher temperature (Fig. 34). The evaporative energy fraction is effective at marginally higher temperature for the west side as compared to east side of the system. It is effective around 25 °C for Al_2O_3-water based nanofluid while for TiO_2 and CuO-water based nanofluid, it is effective at marginally higher temperature range (30 °C − 35 °C). The higher value of the evaporation energy fraction means that the evaporation rate is higher from the water surface. Whereas, higher the convective fraction energy, faster the transfer of evaporated water vapor (due to free convective currents) on the inner surface of the glass cover. Therefore, both these fractions need to be higher to increase the distillate yield and hence energy efficiency.

6. Conclusions

Following conclusions has been withdrawn from the present review:

(a) On the basis of hourly yield, Kumar and Tiwari model (KTM) is superior to the others

model under consideration with least percentage deviation except in extreme cases. It is recommended that before predicting the performance theoretically, the values of *C* and *n* must be carried out experiments for given climatic conditions and for a particular design of the solar still.

(b) The non-linear characteristic equations are found more suitable for the thermal testing of passive and hybrid (PV-T) active solar still.

(c) Passive single slope solar stills perform better than passive double slop solar stills on the basis of annual yield, annual energy, annual exergy and exergoeconomic parameters.

(d) Passive double slope solar stills perform better than passive single slope solar stills on the basis of yield.

(e) On the basis of yield, single slope active solar still integrated with N PVT-FPC performs better than the double slope active solar still integrated with N PVT-FPC if the basin water depth is more than 0.15 m and vice versa if the depth is less than 0.15 m.

(f) Double slope active solar still integrated with N PVT-FPC performs better than single slope active solar still integrated with N PVT-FPC on the basis of exergoeconomic parameter, enviroeconomic parameter, energy matrices and yield at 0.14 m water depth for same basin area ($N = 11, \dot{m}_f = 0.03$ kg/s).

(g) Single slope active solar still integrated with N-PVT-CPC performs better than double slope active solar still integrated with N-PVT-CPC on the basis of yield if depth is more than 0.19 m and vice versa if depth is less than 0.19 m.

(h) It is necessary to adjust the combination between the size of ETC and basin water depth to make the active ETC-SSSS system more efficient. Smaller size of ETC with ten number of tubes is preferable than a single unit the larger size ETC integrated. Optimum mass flow rate of 0.06 kg/s is obtained with water depth of 0.03 m in the basin.

(i) The passive double slope solar stills with Al_2O_3, TiO_3, CuO-water based nanofluids performs better than the passive double slope solar stills without nanofluids on the basis of yield, instantaneous energy and exergy efficiencies.

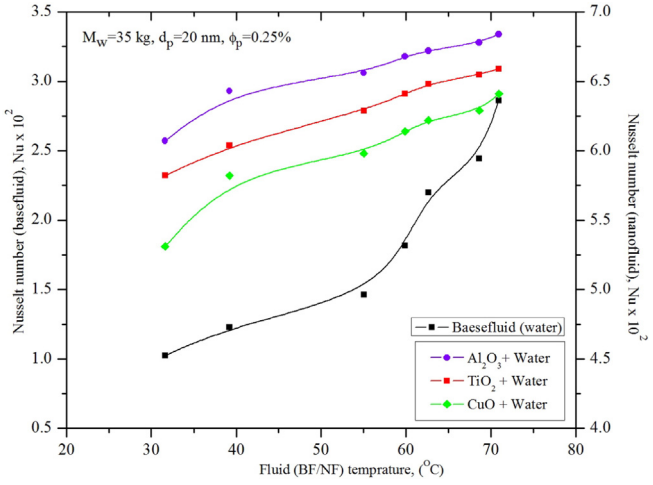

Fig. 32. Variation of Nusselt number with fluid temperature (BF/NF) for basefluid and Al_2O_3, TiO_2, and CuO-water based nanofluids.

Please cite this article as: G.N. Tiwari, L. Sahota, Review on the energy and economic efficiencies of passive and active solar distillation systems, Desalination (2016), http://dx.doi.org/10.1016/j.desal.2016.08.023

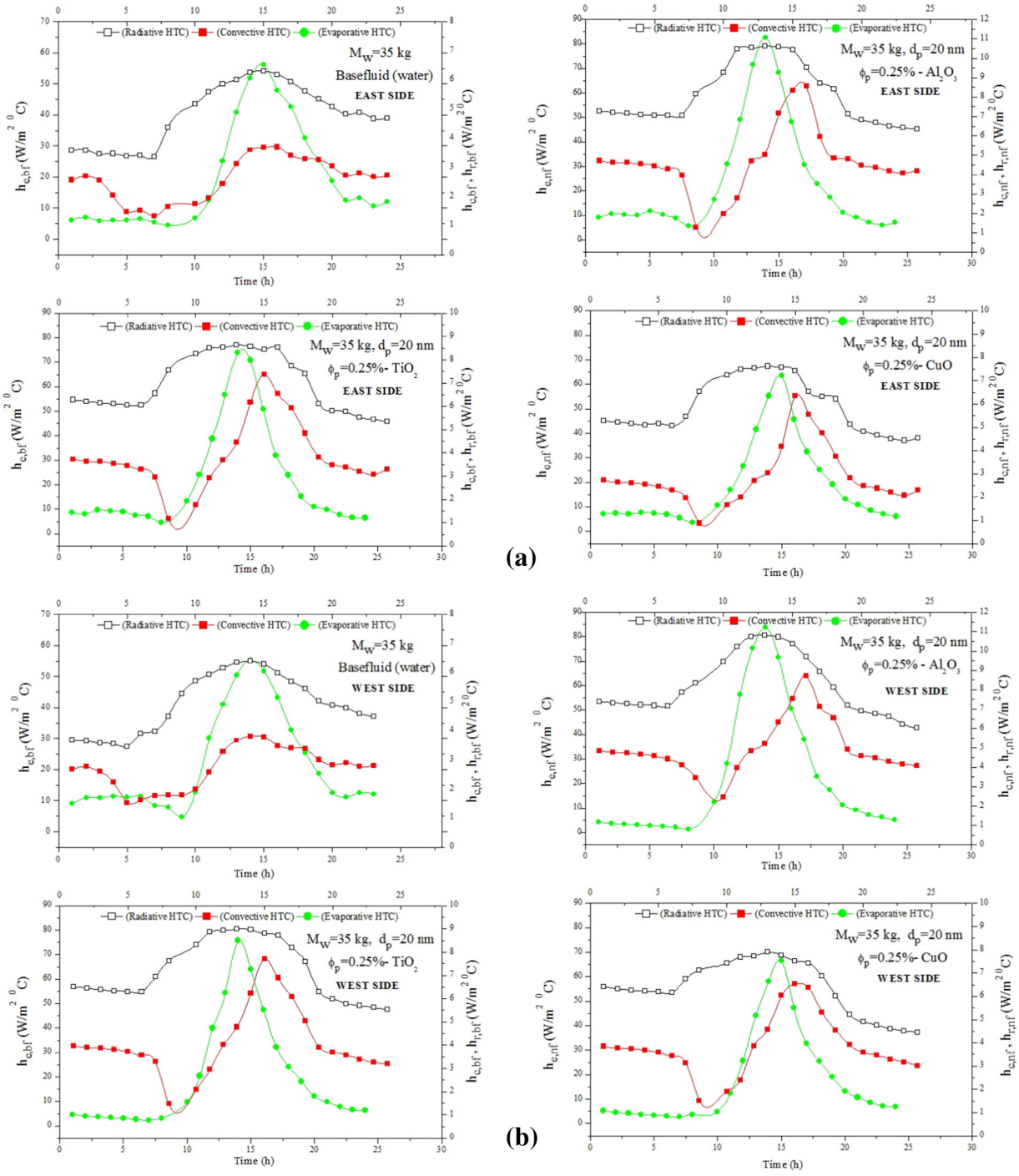

Fig. 33. Hourly variation of internal heat transfer coefficients (evaporative, convective, and radiative) of basefluid (water) and Al_2O_3, TiO_2, and CuO-water based nanofluid for (a) east side and (b) west side of passive DSSS.

7. Scope of future work

Following future work has been recommended on the basis of present review:

(a) The performance of passive and active solar stills with rain water harvesting for a large scale can be studied.

(b) The performance of solar still with different types of PV technology, and with different types of collector assembly can be analyzed.

(c) The effect of different condensing chambers for fast condensation should be analyzed for PVT active slope solar still due to high operating temperature.

(d) The active and passive solar distillation systems can be studied for higher temperature water based nanofluids (metallic nanoparticles having better thermo-physical properties) with heat exchanger.

(e) The design and size of the heat exchanger as per the solar still design and fluid quality (basefluid/nanofluid) can be optimized for a given output.

Please cite this article as: G.N. Tiwari, L. Sahota, Review on the energy and economic efficiencies of passive and active solar distillation systems, Desalination (2016), http://dx.doi.org/10.1016/j.desal.2016.08.023

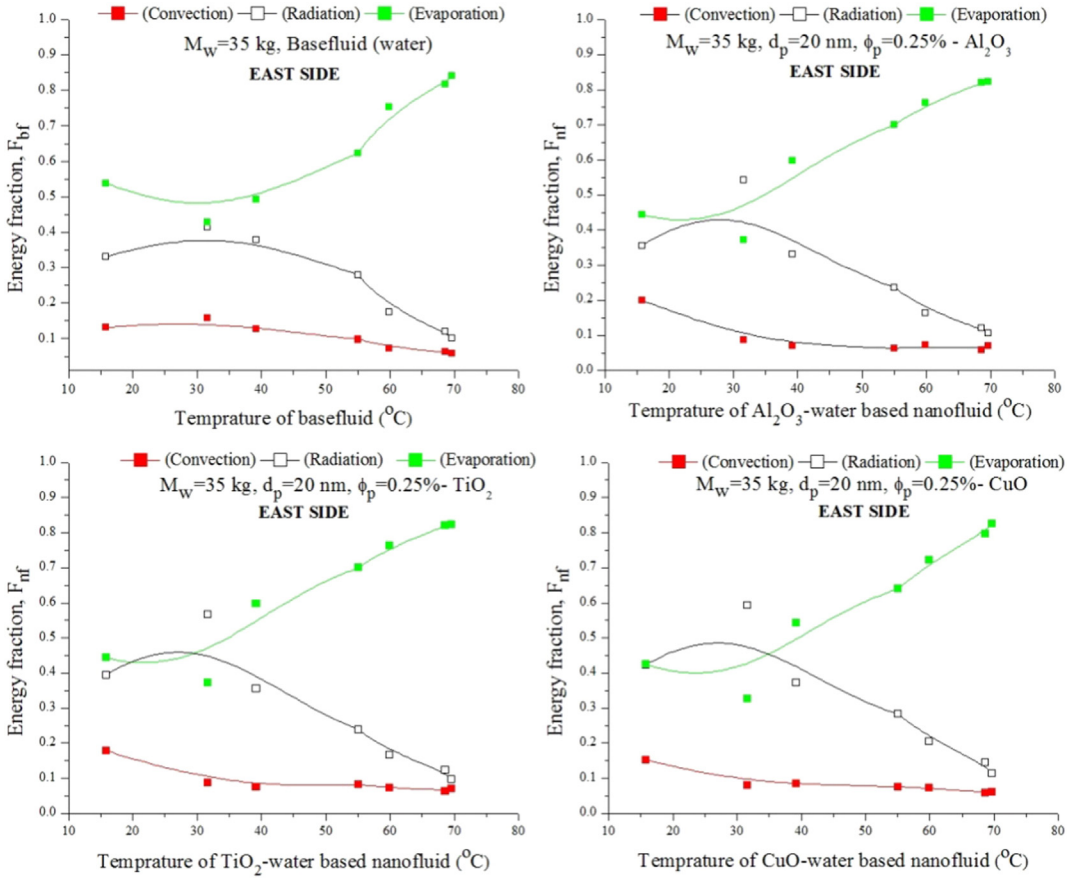

Fig. 34. Variation of Convection, radiation, and evaporation energy fraction of basefluid(water) and Al_2O_3, TiO_2, and CuO-water based nanofluid with temperature of the fluid (BF/NF) for east side of passive DSSS.

(f) Long term performance, life cycle cost analysis, Exergoeconomic and enviroeconomic analysis for all the above cited system can be studied for different climatic conditions.

Nomenclature

A_g = area of the glass cover (m^2)	$I_{SE}(t)$ = solar intensity on the east side (W/m^2)
A_{gE} = area of the east side glass cover (m^2)	$I_{SW}(t)$ = solar intensity on the west side (W/m^2)
A_{gW} = area of the west side glass cover (m^2)	h_{ew} = evaporative heat transfer coefficient from water to glass surface (W/m^2 °C)
A_b = area of the basin (m^2)	h_{rw} = radiative heat transfer coefficient from water to glass surface (W/m^2 °C)
A_c = area of the collector (m^2)	h_{cw} = convective heat transfer coefficient from water to glass surface (W/m^2 °C)
A_m = area of the module (m^2)	h_{1w} = total internal heat transfer coefficient from water to glass surface (W/m^2 °C)
A_t = circumferential area of each tubular absorber (m^2)	h_{bw} = natural convective heat transfer coefficient from basin to water (W/m^2 °C)
A_a = aperture area of solar collector(m^2)	h_b = heat transfer coefficient from basin to ambient (W/m^2 °C)
d_t = diameter of evacuated tube (m)	h_w = wind heat transfer coefficient (W/m^2 °C)
T_w = water temperature (°C)	h_{rg} = radiative heat transfer coefficient from glass to ambient (W/m^2 °C)
T_{wo} = water temperature at time $t=0$ (°C)	h_{cg} = convective heat transfer coefficient from glass to ambient (W/m^2 °C)
T_{gi} = temperature of inner surface of the glass cover (°C)	h_{1g} = total heat transfer coefficient from glass to ambient (W/m^2 °C)
T_{go} = temperature of outer surface of the glass cover (°C)	h_{rgE} = radiative heat transfer coefficient from the east side glass to ambient (W/m^2 °C)

(*continued*)

A_g = area of the glass cover (m^2)	$I_{SE}(t)$ = solar intensity on the east side (W/m^2)
T_b = temperature of basin surface (°C)	h_{rgW} = radiative heat transfer coefficient from the west side glass to ambient (W/m^2 °C)
T_a = ambient temperature (°C)	h_{1wE} = total heat transfer coefficient from the water surface to east side glass cover (W/m^2 °C)
T_s = Sun. temperature (°C), T_{sky} = sky temperature (°C)	h_{1wW} = total heat transfer coefficient from the water surface to west side glass cover (W/m^2 °C)
T_t = collector tube temperature (°C)	$h_{1bf,E}$ = total heat transfer coefficient from the bsefluid surface to east side glass cover (W/m^2 °C)
T_{cw} = water temperature in evacuated tubular collector (°C)	$h_{1bf,W}$ = total heat transfer coefficient from the bsefluid surface to west side glass cover (W/m^2 °C)
T_{sw} = water temperature in still (°C)	$h_{b,bf}$ = heat transfer coefficient from basin to basefluid (W/m^2 °C)
T_{giE} = temperature of inner surface of the east side glass cover (°C)	$h_{b,bf}$ = heat transfer coefficient from basin to basefluid (W/m^2 °C)
T_{giW} = temperature of inner surface of the west side glass cover (°C)	$h_{ebf,E}$ = evaporative heat transfer coefficient from basefluid to east side glass cover (W/m^2 °C)
T_{goE} = temperature of outer surface of the east side glass cover (°C)	$h_{ebf,W}$ = evaporative heat transfer coefficient from basefluid to west side glass cover (W/m^2 °C)
T_{goW} = temperature of outer surface of the west side glass cover (°C)	h_{nc} = natural convective heat transfer coefficient from basin to basefluid (W/m^2 °C)
T_{bf} = basefluid temperature (°C)	h_{tw} = heat transfer coefficient between tube and water (W/m^2 °C)

Please cite this article as: G.N. Tiwari, L. Sahota, Review on the energy and economic efficiencies of passive and active solar distillation systems, Desalination (2016), http://dx.doi.org/10.1016/j.desal.2016.08.023

(*continued*)

A_g = area of the glass cover (m^2)	$I_{SE}(t)$ = solar intensity on the east side (W/m^2)
$I(t)$ = solar intensity (W/m^2)	h_{ta} = heat transfer coefficient between collector tube and ambient (W/m^2 °C)
$I_s(t)$ = solar intensity on the still (W/m^2)	U_{cg-a} = overall heat transfer coefficient from inner surface of glass to ambient (W/m^2 °C)
$I_c(t)$ = solar intensity on the collector (W/m^2)	U_r = total heat transfer coefficient from basin to
ambient (W/m^2 °C)	$\dot{Q}_u$ = usefull thermal energy gain from collector (W/m^2)
U_L = overall heat transfer coefficient through the still (W/m^{2}°C)	$\dot{Q}_{uth,N}$ = usefull thermal energy gain from N-collectors (W/m^2)
K_g = thermal conductivity of glass (W/m °C)	$\dot{q}_{eE}$ =rate of evaporative heat transfer from the east side (W/m^2)
K_g = thickness of glass cover (m)	$\dot{q}_{eW}$ =rate of evaporative heat transfer from the west side (W/m^2))
$M_{sw} = M_w$ = water mass in still (kg), $\dot{M}_w$ = yield (kg)	$\dot{q}_{1w}$ =rate of total heat transfer from water to glass cover (W/m^2)
M_{bf} = basefluid mass in the still (kg)	$\dot{q}_{1w}$ =rate of total heat transfer from basefluid to glass cover (W/m^2)
M_{cw} = water mass in evacuated tubular collector (kg)	$\dot{q}_{eW}$ =rate of evaporative heat transfer (W/m^2)
N_c = number of tubes in collector	$\overline{f(t)}$ = average value of $f(t)$ for time interval Δt
C_{bf} = specific heat capacity of basefluid (J/kg K)	ϵ_i = instantaneous thermal exergy efficiency
L = latent heat of vaporization (J/kg)	$\dot{E}_{X,evap}$ =evaporative exergy flow rate (W)
Gr = Grashof number, Pr = Prandtl number	$\dot{E}_{X,Sun}$ =rate of exergy input from the Sun (W)
Re = Reynold's number	$\dot{E}_{X,cw}$ =convective exergy flow rate from water to glass cover (W)
K_v = thermal conductivity of humid air (W/m °C)	$\dot{E}_{X,rw}$ =radiative exergy flow rate from water to glass cover (W)
X_v = characteristic length between water and glass surface (m)	F_{eX} = evaporative fraction exergy
V_{OC} = open circuit voltage (V)	F_{cX} = convective fraction exergy
I_{SC} = short circuit current (A), FF = fill factor	F_{rX} = radiative fraction exergy
I_C = load current (A), V_L = load voltage (V)	P = partial vapor pressue (Pa)
$\dot{m}$ = natural circulation rate via discrete tubes (kg/s)	Δt = time interval
r_{inv} = reflectivity of reflector under the still	

Greek letters

τ_w = transmitivity of the water	α_b = absorptivity of the basin
τ_g = transmitivity of the glass	α_t = absorptivity of the tube
ϵ_g = transmitivity of the glass	ρ_r = reflectivity of the reflector plate
α_w = absorptivity of the water	η_i = instantaneous thermal efficiency
σ = Stefan Boltzmann constant, 5.6697×10^{-8} (W/m^2 K^4)	η_{iL} = instantaneous thermal loss efficiency
α_g = absorptivity of the glass	

Abbreviations

HTC	heat transfer coefficient	PVT	photovoltaic thermal
SSSS	single slope solar still	FPC	flat plate collector
DSSS	double slope solar still	UAC	uniform annual cost
IASS	inverted absorber solar still	CPK	cost of distilled water per kg
CPC	compound parabolic concentrator	EPBT	energy payback time
FRP	Fibre reinforced plastic	BF/bf	basefluid
ETC	evacuated tubular collector	NF/nf	nanofluid

References

[1] G. Nebbia, G.N. Menozzi, Historical aspects of dissalzione, Acqua Ind. 41–42 (1966) 3–20.
[2] H.P. Garg, H.S. Mann, Effect of climatic, operational and design parameters on the year round performance of single sloped and double sloped solar still under Indian arid zone conditions, Sol. Energy 18 (1976) 159–163.
[3] M.A.S. Malik, G.N. Tiwari, A. Kumar, M.S. Sodha, Solar Distillation, Pergamon Press, Oxford, UK, 1982.
[4] H.S. Soliman, Solar still Coupled with a Solar Water Heater, Mosul University, Mosul, Iraq, 1976.
[5] M.S. Sodha, A. Kumar, G.N. Tiwari, R.C. Tyagi, Simple multiple wick solar still: analysis and performance, Sol. Energy 26 (1981) 127–131.
[6] S.N. Rai, G.N. Tiwari, Single basin solar still coupled with flat plate collector, Energy Convers. Manag. 23 (1983) 145–149.
[7] G.N. Tiwari, S.B. Sharma, M.S. Sodha, Performance of double condensing cover multi wick solar still, Energy Convers. Manag. 24 (1984) 155–159.
[8] G.N. Tiwari, H.P. Garg, Studies on various designs of solar distillation systems, Solar & Wind Technology 1 (1985) 161–165.
[9] G.N. Tiwari, Y.P. Yadav, Comparative designs and long term performance of various designs of solar distillery, Energy Convers. Manag. 27 (1987) 327–333.
[10] S.A. Lawrence, G.N. Tiwari, Theoretical evaluation of solar distillation under natural circulation with heat exchanger, Energy Convers. Manag. 30 (1990) 205–213.
[11] A.M. Tayeb, Performance studies of some designs of solar stills, Energy Convers. Manag. 33 (1992) 889–898.
[12] G.N. Tiwari, Recent advances in solar distillation, in: K. Raj, K.P. Maheshwari, R.L. Sawhney (Eds.), International Journal of Solar Energy and Energy Conservation, Chapter 2, Wiley Eastern, New Delhi 1992, pp. 32–149.
[13] G.N. Tiwari, H.N. Singh, R. Tripathi, Present status of solar distillation, Sol. Energy 75 (2003) 367–373.
[14] R. Tripathi, G.N. Tiwari, Effect of water depth on internal heat and mass transfer for active solar distillation, Desalination 173 (2005) 187–200.
[15] A.K. Tiwari, G.N. Tiwari, Effect of water depths on heat and mass transfer in a passive solar still: in summer climatic condition, Desalination 195 (2006) 78–94.
[16] A.K. Tiwari, G.N. Tiwari, Thermal modeling based on solar fraction and experimental study of the annual and seasonal performance of a single slope passive solar still: the effect of water depths, Desalination 207 (2007) 184–204.
[17] P.T. Tsilingiris, The influence of binary mixture thermo-physical properties in the analysis of heat and mass transfer processes in solar distillation systems, Sol. Energy 81 (2007) 1482–1491.
[18] P.T. Tsilingiris, Modeling heat and mass transport phenomena at higher temperatures in solar distillation systems – the Chilton–Colburn analogy, Sol. Energy 84 (2010) 308–317.
[19] P.T. Tsilingiris, Combined heat and mass transfer analyses in solar distillation systems – the restrictive conditions and a validity range investigation, Sol. Energy 86 (2012) 3288–3300.
[20] P.T. Tsilingiris, Theoretical derivation and comparative evaluation of mass transfer coefficient modeling in solar distillation systems – the Bowens ratio approach, Sol. Energy 112 (2015) 218–231.
[21] V.K. Dwivedi, G.N. Tiwari, Comparison of internal heat transfer coefficients in passive solar stills by different thermal models: an experimental validation, Desalination 246 (2009) 300–318.
[22] G.N. Govind, Tiwari, Economic analysis of some solar energy systems, Energy Conversion Management 24 (1984) 131–135.
[23] K. Mukherjee, G.N. Tiwari, Economic analysis of various designs of conventional solar stills, Energy Convers. Manag. 26 (1986) 155–157.
[24] S. Kumar, G.N. Tiwari, Life cycle cost analysis of single slope hybrid (PV/T) active solar still, Appl. Energy 86 (2009) 1995–2004.
[25] X. Liu, W. Chen, M. Gu, S. Shen, G. Cao, Thermal and economic analyses of solar desalination system with evacuated tubular collectors, Sol. Energy 93 (2013) 144–150.
[26] E. El-Bialy, S.M. Shalaby, A.E. Kabeel, A.M. Fathy, Cost analysis for several solar desalination systems, Desalination 384 (2016) 12–30.
[27] T. Arunkumar, R. Jayaprakash, D. Denkenberger, A. Ahsan, M.S. Okundamiya, K.S. Kumar, H. Tanaka, H.S. Aybar, An experimental study on a hemispherical solar still, Desalination 286 (2012) 342–348.
[28] R. Jayaprakash, K. Perumal, T. Arunkumar, S. Kumar, B. Selvakumar, Design and performance analysis of low cost solar still using transparent LDPE cover, Journal of Environmental Research and Development 4 (2009) 465–475.
[29] R. Sathyamurthy, H.J. Kennady, P.K. Nagarajan, A. Ahsan, Factors affecting the performance of triangular pyramid solar still, Desalination 344 (2014) 383–390.
[30] T. Rajaseenivasan, K.K. Murugavel, Theoretical and experimental investigation on double basin double slope solar still, Desalination 319 (2013) 25–32.
[31] P.U. Suneesh, R. Jayaprakash, T. Arunkumar, D. Denkenberger, Effect of air flow on "V" type solar still with cotton gauze cooling, Desalination 337 (2014) 1–5.
[32] H.E. Gad, S.S. El-Din, A.A. Hussien, K. Ramzy, Thermal analysis of a conical solar still performance: an experimental study, Sol. Energy 122 (2015) 900–909.
[33] A.E. Kabeel, Performance of solar still with a concave wick evaporation surface, Energy 34 (2009) 1504–1509.
[34] H.S. Aybar, F. Egelioglu, U. Atikol, An experimental study on an inclined solar water distillation system, Desalination 180 (2005) 285–289.
[35] H. Tanaka, Tilted wick solar still with flat plate bottom reflector, Desalination 273 (2011) 405–413.
[36] A.S. Abdullah, Improving the performance of stepped solar still, Desalination 319 (2013) 60–65.

Please cite this article as: G.N. Tiwari, L. Sahota, Review on the energy and economic efficiencies of passive and active solar distillation systems, Desalination (2016), http://dx.doi.org/10.1016/j.desal.2016.08.023

[37] A.E. Kabeel, A. Khalil, Z.M. Omara, M.M. Younes, Theoretical and experimental parametric study of modified stepped solar still, Desalination 289 (2012) 12–20.
[38] T. Hiroshi, Tilted wick solar still with external flat plate reflector: optimum inclination of still and reflector, Desalination 249 (2009) 411–415.
[39] H. Tanaka, Tilted wick solar still with flat plate bottom reflector, Desalination 273 (2011) 405–413.
[40] O. Ansari, M. Asbik, A. Bah, A. Arbaoui, A. Khmou, Desalination of the brackish water using a passive solar still with a heat energy storage system, Desalination 324 (2013) 10–20.
[41] F.T. Farshad, M. Dashtban, M. Hamid, Experimental investigation of a weir-type cascade solar still with built-in latent heat thermal energy storage system, Desalination 260 (2010) 248–253.
[42] T. Arunkumar, D. Denkenberger, A. Ahsan, R. Jayaprakash, The augmentation of distillate yield by using concentrator coupled solar still with phase change material, Desalination 314 (2013) 189–192.
[43] A. Ahsan, T. Fukuhara, Mass and heat transfer model of Tubular Solar Still, Sol. Energy 84 (2010) 1147–1156.
[44] K. Murase, H. Tobata, M. Ishikawa, S. Toyama, Experimental and numerical analysis of a tube-type networked solar still for desert technology, Desalination 190 (2006) 137–146.
[45] S. Gorjian, B. Ghobadian, T.T. Hashjin, A. Banakar, Experimental performance evaluation of a stand-alone point-focus parabolic solar still, Desalination 352 (2014) 1–17.
[46] H.E.S. Fath, S.M. Elsherbiny, Effect of adding a passive condenser on solar still performance, Energy Convers. Manag. 34 (1993) 63–73.
[47] P.V. Kmar, A. Kumar, O. Prakash, A.K. Kaviti, Solar stills system design: a review, Renewable and Sustainable Energy Reviews 51 (2015) 153–181.
[48] C. Elango, N. Gunasekaran, K. Sampathkumar, Thermal models of solar still - a comprehensive review, Renew. Sust. Energ. Rev. 47 (2015) 856–911.
[49] G.N. Tiwari, R.K. Mishra, Advanced Renewable Energy Sources, RSC Publishing Cambridge, UK, 2012.
[50] R.V. Dunkle, Solar water distillation, the roof type solar still and a multi effect diffusion still, International Developments in Heat Transfer, ASME, Proceeding, International Journal of Heat Transfer, 895, University of Colorado, 1961 Part V.
[51] S. Kumar, G.N. Tiwari, Estimation of convective mass transfers in solar distillation system, Sol. Energy 57 (1996) 459–464.
[52] Z. Chen, X. Ge, X. Sun, L. Bar, Y.X. Miao, Natural convection heat transfer across air layers at various angles of inclination, Engineering Thermo physics (1984) 211–220.
[53] R.S. Adhikari, A. Kumar, A. Kumar, Estimation of mass transfer rates in solar stills, Int. J. Energy Res. 14 (1990) 737–744.
[54] H. Zheng, X. Zhang, J. Zhang, Y. Wu, A group of improved heat and mass transfer correlations in solar stills, Energy Convers. Manag. 43 (2001) 2469–2478.
[55] R. Dev, G.N. Tiwari, Characteristic equation of passive solar still, Desalination 245 (2009) 246–265.
[56] R. Dev, H.N. Singh, G.N. Tiwari, Characteristic equation of double slope passive solar still, Desalination 267 (2011) 261–266.
[57] G.N. Tiwari, M.A. Noor, Characteristic equation of solar still, Sustainable Energy 18 (1996) 147–171.
[58] R. Dev, G.N. Tiwari, Characteristic equation of the inverted absorber solar still, Desalination 269 (2011) 67–77.
[59] S. Kumar, G.N. Tiwari, Analytical expression for instantaneous exergy efficiency of a shallow basin passive solar still, Int. J. Therm. Sci. 50 (2011) 2543–2549.
[60] S. Kumar, G.N. Tiwari, Estimation of internal heat transfer coefficients of a hybrid (PV/T) active solar still, Sol. Energy 83 (2009) 1656–1667.
[61] S. Kumar, G.N. Tiwari, M.K. Gaur, Development of empirical relation to evaluate the heat transfer coefficients and fractional energy in basin type hybrid (PV/T) active solar still, Desalination 250 (2010) 214–221.
[62] R. Dev, G.N. Tiwari, Characteristic equation of a hybrid (PV-T) active solar still, Desalination 254 (2010) 126–137.
[63] V.K. Dwivedi, G.N. Tiwari, Experimental validation of thermal model of a double slope active solar still under natural circulation mode, Desalination 250 (2010) 49–55.
[64] M.K. Gaur, G.N. Tiwari, Optimization of number of collectors for integrated PV/T hybrid active solar still, Appl. Energy 87 (2010) 1763–1772.
[65] S. Dubey, G.N. Tiwari, Thermal modeling of a combined system of photovoltaic thermal (PV/T) solar water heater, Sol. Energy 82 (2008) 602–612.
[66] G. Singh, S. Kumar, G.N. Tiwari, Design, fabrication and performance evaluation of a hybrid photovoltaic thermal (PVT) double slope active solar still, Desalination 277 (2011) 399–406.
[67] G.N. Tiwari, J.K. Yadav, D.B. Singh, I.M. Al-Helal, A.M. Abdel-Ghany, Exergoeconomic and enviroeconomic analyses of partially covered photovoltaic flat plate collector active solar distillation system, Desalination 367 (2015) 186–196.
[68] B.K. Sovacool, Valuing the greenhouse gas emissions from nuclear power: a critical survey, Energ Policy 36 (2008) 2940–2953.
[69] H. Caliskan, I. Dincer, A. Hepbasli, Exergoeconomic, enviroeconomic and sustainability analyses of a novel air cooler, Energy Buildings 55 (2012) 747–756.
[70] C.S. Rajoria, S. Agrawal, G.N. Tiwari, Exergetic and enviroeconomic analysis of novel hybrid PVT array, Sol. Energy 88 (2013) (2012) 110–119.
[71] P.K. Nag, Basic and Applied Thermodynamics, Tata McGraw-Hill, 2004 ISBN 0-07-047338-2.
[72] G.N. Tiwari, M.K. Ghosal, Renewable Energy Resources: Basic Principles and Applications, Narosa Publishing House, New Delhi, 2005.
[73] G.N. Tiwari, Solar Energy: Fundamentals, Design, Modelling and Applications, CRC Publication/Narosa Publishing House, New Delhi/New York, 2002.
[74] S. Kumar, A. Tiwari, Design, fabrication and performance of a hybrid photovoltaic/thermal (PV/T) active solar still, Energy Convers. Manag. 51 (2010) 1219–1229.
[75] D.B. Singh, J.K. Yadav, V.K. Dwivedi, S. Kumar, G.N. Tiwari, I.M. Al-Helal, Experimental studies of active solar still integrated with two hybrid PVT collectors, Sol. Energy 130 (2016) 207–223.
[76] S. Kumar, G.N. Tiwari, Life cycle cost analysis of single slope hybrid (PV/T) active solar still, Appl. Energy 86 (2009) 1995–2004.
[77] R.V. Singh, S. Kumar, M.M. Hasan, M.E. Khan, G.N. Tiwari, Performance of a solar still integrated with evacuated tubular collector in natural mode, Desalination 318 (2013) 25–33.
[78] S. Kumar, A. Dubey, G.N. Tiwari, A solar still augmented with an evacuated tubular collector in forced mode, Desalination 347 (2014) 15–24.
[79] M. Edalatpour, A. Kianifar, G.N. Tiwari, O. Mahiana, K. Aryana, S. Wongwises, Solar stills: a review of the latest developments in numerical simulations, Sol. Energy 135 (2016) 897–922.
[80] A.A. El-Sebaii, M.R.I. Ramadan, S. Aboul-Enein, M. El-Naggar, Effect of fin configuration on single slope solar still performance, Desalination 365 (2015) 15–24.
[81] S.P. Srivastava, S.K. Agrawal, Experimental and theoretical analysis of single sloped basin type solar still consisting of multiple low thermal inertia floating porous absorbers, Desalination 311 (2013) 198–205.
[82] M. Zerrouki, N. Settou, Y. Marif, M.M. Belhadj, Simulation study of a capillary film solar still coupled with a conventional solar still in south Algeria, Energy Convers. Manag. 85 (2014) 112–119.
[83] T. Rajaseenivasan, Kalidasa, K.K. Murugavel, T. Elango, R.S. Hansen, A review of different methods to enhance the productivity of the multi-effect solar still, Renewable and Sustainable Energy 474 Reviews 17 (2013) 248–259.
[84] T. Abderachid, K. Abdenacer, Effect of orientation on the performance of a symmetric solar still with a double effect solar still (comparison study), desalination 329 (2013) 68–77
[85] A.E. Kabeel, A. Khalil, Z.M. Omara, M.M. Younes, Theoretical and experimental parametric study of modified stepped solar still, Desalination 289 (2012) 12–20.
[86] Z.M. Omara, A.E. Kabeel, M.M. Younes, Enhancing the steeped solar still performance using internal reflectors, Desalination 314 (2013) 67–72.
[87] N. Rahbar, J.A. Esfahani, E. Fotouhi-Bafghi, Estimation of convective heat transfer coefficient and water productivity-yield in a tubular solar still-CFD simulation and theoretical analysis, Sol. Energy 113 (2015) 313–323.
[88] K.S. Reddy, K. Ravi Kumar, T.S. O'Donovan, T.K. Mallick, Performance analysis of an evacuated multi-stage solar water desalination system, Desalination 288 (2012) 80–92.
[89] J. Xiong, G. Xie, H. Zheng, Experimental and numerical study on a new multi-effect solar still with enhanced condensation surface, Energy Convers. Manag. 73 (2013) 176–185.
[90] G. Xie, J. Xiong, H. Liu, B. Xu, H. Zheng, Y. Yang, Experimental and numerical investigation on a novel solar still with vertical ripple surface, Energy Convers. Manag. 98 (2015) 151–160.
[91] M. Dashtban, F.F. Tabrizi, Thermal analysis of a weir-type cascade solar still integrated with PCM storage, Desalination 279 (2011) 415–422.
[92] F.B. Ziabari, A.Z. Sharak, H. Moghadam, F.F. Tabrizi, Theoretical and experimental study of cascade solar stills, Sol. Energy 90 (2013) 205–211.
[93] M.I.M. Shatat, K. Mahkamov, Determination of rational design parameters of a multi-stage solar water desalination still using transient mathematical modelling, Renew. Energy 35 (2010) 52–61.
[94] P. Monowe, M. Masale, N. Nijegorodov, V. Vasilenko, A portable single-basin solar still with an external reflecting booster and an outside condenser, Desalination 280 (2011) 332–338.
[95] V.G. Gude, N. Nirmalakhandan, S. Deng, A. Maganti, Low temperature desalination using solar collectors augmented by thermal energy storage, Appl. Energy 91 (2012) 466–474.
[96] Z.M. Omara, M.A. Eltawil, E.A. Elnashar, A new hybrid desalination system using wicks/solar still and evacuated solar water heater, Desalination 325 (2013) 56–64.
[97] X. Liu, W. Chen, M. Gu, S. Shen, G. Cao, Thermal and economic analyses of solar desalination system with evacuated tubular collectors, Sol. Energy 93 (2013) 144–150.
[98] R. Kannan, C. Selvaganesan, M. Vignesh, B.R. Babu, M. Fuentes, M. Vivar, I. Skryabin, K. Srithar, Solar still with vapor adsorption basin: performance analysis, Renew. Energy 62 (2014) 258–264.
[99] M. Al-Nimr, M.E. Dahdolan, Modeling of a novel concentrated solar still enhanced with a porous evaporator and an internal condenser, Sol. Energy 114 (2015) 8–16.
[100] H. Sharon, K.S. Reddy, Performance investigation and enviro-economic analysis of active vertical solar distillation units, Energy 84 (2015) 794–807.
[101] G.N. Tiwari, R.K. Mishra, Advanced Renewable Energy Sources, RSC Publishing, Cambridge, UK, 2012.
[102] L. Sahota, G.N. Tiwari, Effect of Al_2O_3 nanoparticles on the performance of passive double slope solar still, Sol. Energy 130 (2016) 260–272.
[103] L. Sahota, G.N. Tiwari, Effect of nanofluids on the performance of passive double slope solar still: a comparative study using characteristic curve, Desalination 388 (2016) 9–21.
[104] L. Sahota, G.N. Tiwari, Effect of aluminium oxide and titanium oxide -water based nanofluid on heat transfer coefficients of passive double slope solar still, Int. J. Energy Environ. Econ. 24 (1) (2016).
[105] D.B. Singh, G.N. Tiwari, Effect of energy matrices on life cycle cost analysis of partially covered photovoltaic compound parabolic concentrator collector active solar distillation system, Desalination 397 (2016) 75–91.
[106] D.B. Singh, G.N. Tiwari, I.M. Al-Helal, V.K. Dwivedi, J.K. Yadav, Effect of energy matrices on life cycle cost analysis of passive solar stills, Sol. Energy 134 (2016) 9–22.
[107] International Labor Office, Introduction to Work Study, International Labor Organization, Geneva, 1979 ISBN 81-204-0602-8.

Please cite this article as: G.N. Tiwari, L. Sahota, Review on the energy and economic efficiencies of passive and active solar distillation systems, Desalination (2016), http://dx.doi.org/10.1016/j.desal.2016.08.023

[108] C. Popiel, J. Wojtkowiak, Simple formulas for thermo-physical properties of liquid water for heat transfer calculations (from 0 °C to 150 °C), Heat Transfer Engineering 19 (1998) 87–101.
[109] B.C. Pak, Y.I. Cho, Hydrodynamic and heat transfer study of dispersed fluids with submicron metallic oxide particles, Experimental Heat Transfer 11 (1998) 151–170.
[110] K. Khanafer, K. Vafai, A critical synthesis of thermo-physical characteristics of nanofluids, Int. J. Heat Mass Transf. 54 (2011) 4410–4428.
[111] K.S. Wang, J.H. Lee, S.P. Jang, Buoyancy-driven heat transfer of water-based Al_2O_3 nanofluids in a rectangular cavity, Int. J. Heat Mass Transf. 50 (2007) 4003–4010.
[112] C.J. Ho, M.W. Chen, Z.W. Li, Numerical simulation of natural convection of nanofluid in a square enclosure: effects due to uncertainties of viscosity and thermal conductivity, Int. J. Heat Mass Transf. 51 (2008) 4506–4516.

Please cite this article as: G.N. Tiwari, L. Sahota, Review on the energy and economic efficiencies of passive and active solar distillation systems, Desalination (2016), http://dx.doi.org/10.1016/j.desal.2016.08.023